General Disclaimer

One or more of the Following Statements may affect this Document

- This document has been reproduced from the best copy furnished by the organizational source. It is being released in the interest of making available as much information as possible.

- This document may contain data, which exceeds the sheet parameters. It was furnished in this condition by the organizational source and is the best copy available.

- This document may contain tone-on-tone or color graphs, charts and/or pictures, which have been reproduced in black and white.

- This document is paginated as submitted by the original source.

- Portions of this document are not fully legible due to the historical nature of some of the material. However, it is the best reproduction available from the original submission.

X-695-77-30
PREPRINT

TMX-71314

MAGNETOSHEATH ELECTROSTATIC TURBULENCE

PAUL RODRIGUEZ

FEBRUARY 1977

GSFC — GODDARD SPACE FLIGHT CENTER —
GREENBELT, MARYLAND

MAGNETOSHEATH ELECTROSTATIC TURBULENCE

by

Paul Rodriguez*

Planetary Sciences Branch
Laboratory for Extraterrestrial Physics
NASA/Goddard Space Flight Center
Greenbelt, Maryland 20771

* University of Maryland Research Associate

ABSTRACT

Using measurements obtained with the University of Iowa plasma wave experiment on the IMP-6 satellite, a study has been conducted of the spectrum of electrostatic plasma waves in the terrestrial magnetosheath. Electrostatic plasma wave turbulence is almost continuously present throughout the magnetosheath with broadband (20 Hz - 70 kHz) r.m.s. field intensities typically 0.01 - 1.0 millivolts m^{-1}. Peak intensities of about 1.0 millivolts m^{-1} near the electron plasma frequency (30 - 60 kHz) have been detected occasionally. Two or three components can usually be identified in the spectrum of magnetosheath electrostatic turbulence: a high frequency ($\geq$ 30 kHz) component peaking at the electron plasma frequency f_{pe}, a low frequency component with a broad intensity maximum below the nominal ion plasma frequency f_{pi} ($\sim f_{pe}/43$), and a less well defined intermediate component in the range $f_{pi} < f < f_{pe}$. The intensity distribution of magnetosheath electrostatic turbulence clearly shows that the low frequency component is associated with the bow shock, suggesting that the ion heating begun at the shock continues into the downstream magnetosheath. Electrostatic waves below 1 kHz are polarized along the magnetic field direction, a result consistent with the polarization of electrostatic waves at the shock. The high and intermediate frequency components are features of the magnetosheath spectrum which are not characteristic of the shock spectrum, but are often detected in the upstream solar wind. The intensity distribution of electrostatic turbulence at the magnetosheath plasma frequency has no apparent correlation with the shock, indicating that electron plasma oscillations are a general feature of the magnetosheath. The electron plasma frequency shows a tendency to decrease toward the dawn and dusk regions, consistent with a general decrease in electron density away from the subsolar

magnetosheath. Occasionally, intense electrostatic bursts occur which are correlated with magnetic field gradients and fluctuations, possibly indicating the presence of strong current systems, such as can occur at the magnetopause.

INTRODUCTION

A quasi-steady state level of electrostatic plasma wave turbulence characterizes the earth's magnetosheath. Electric field measurements using the long wire antennas on the IMP-6 spacecraft show that electrostatic plasma wave turbulence in the magnetosheath retains some properties associated with the bow shock and displays some new features not usually detected at the bow shock, but which correspond to plasma wave phenomena which occur in the solar wind upstream of the bow shock. For example, electron plasma oscillations are often detected in the solar wind near the earth, apparently resulting from the emission of superthermal electron beams by the bow shock (Scarf et al., 1971; Fredricks et al., 1972; Rodriguez and Gurnett, 1975). As shown below, electron plasma oscillations are also a common feature of the magnetosheath plasma wave spectrum, though it is not yet known whether the bow shock emits superthermal electrons into the magnetosheath. If electron acceleration into the magnetosheath by the bow shock occurs, then it becomes possible to study and compare the wave-particle and wave-wave interactions which occur in the two solar wind states (shocked and unshocked). Thus, on the upstream side, a supersonic plasma is available with $Te/Tp \geq 1$ and $n = n_o$ while on the downstream side, a subsonic plasma exists with $Te/Tp < 1$ and $n \sim 2\ n_o$, where Te and Tp are the electron and proton temperatures and n_o is the upstream particle density. Measurements of magnetosheath particle distributions (Montgomery et al., 1970; Scudder et al., 1973) have revealed numerous nonthermal features in the distributions such as flat-topped electron velocity distributions and high energy

proton beams. The origin and stability properties of such features are so far undetermined. The close association between plasma wave turbulence and the heating and acceleration of the solar wind plasma at the bow shock has been discussed before (Fredricks et al., 1970; Rodriguez and Gurnett, 1975, 1976). It is expected that similarly important effects occur in the magnetosheath since the level of electrostatic plasma wave turbulence remains significant (about an order of magnitude below the levels of electrostatic turbulence at the bow shock, i.e. $\sim$ 1 millivolts m^{-1} r.m.s. in the range 20 Hz - 70 kHz). This report will present the results of a study which suggests that magnetosheath electrostatic turbulence is maintained by the nonthermal features of the particle distributions.

The University of Iowa plasma wave experiment on the IMP-6 spacecraft measured both electric and magnetic field fluctuations with two 16-channel spectrum analyzers which cover the frequency range from 20 Hz to 200 kHz. The basic measurement is a snapshot of the plasma wave spectrum every 5.12 seconds, consisting of an average (AV) spectrum with a 5.12-s time constant, and a peak (PK) spectrum having a 0.1-s time constant. For the present study, the average measurements of the plasma wave spectrum have been further time-averaged to obtain 5.46-min averages; the peak measurements have been further peak-selected to obtain the largest peak measurements over 5.46 minutes. A more detailed description of the IMP-6 plasma wave experiment is given in Rodriguez and Gurnett (1975). The orbit of the IMP-6 spacecraft had an apogee of about 34 R_e, an initial perigee of 1.05 R_e, a period of about 4 days, and an inclination to the ecliptic plane of about 30^o. The spacecraft spent from one to five hours in

the subsolar magnetosheath during both inbound and outbound legs of the orbit; in the dawn and dusk regions of the magnetosheath, the spacecraft was in the magnetosheath for as long as three days. The spacecraft orbit provided full local time coverage (24 hours) in a one year period, or about 90 orbits of the spacecraft.

CHARACTERISTIC MAGNETOSHEATH ELECTROSTATIC SPECTRUM

Measurements of the spectrum of both electric and magnetic field fluctuations in the magnetosheath in the range 20 Hz - 70 kHz show that above about 1 kHz ($\sim f_{ge}$, the electron gyrofrequency) only a fluctuation electric field is usually detected and its polarization confirms the field to be almost completely electrostatic. Below about 1 kHz, narrow band electromagnetic whistler waves (Smith and Tsurutani, 1976) contribute to the measured electric field; however, polarization measurements below 1 kHz again show that the broad band electric field is primarily electrostatic. In addition, the ratio of electric field to magnetic field energy densities $\epsilon_E/\epsilon_B \sim 10^{-1}$-$10^{-2}$ is generally greater than would occur for purely electromagnetic whistler waves (where $\epsilon_E = E^2/8\pi$ and $\epsilon_B = B^2/8\pi$, with E and B the whistler fluctuation electric and magnetic fields, respectively). Even though the electric field spectra to be discussed may show evidence of the narrow band, low frequency noise associated with whistlers, both detailed and averaged measurements support the identification of the broad band electric field observations as electrostatic plasma waves. Whistlers, a ubiquitous phenomenon in the magnetosheath, are not considered in this report.

In general, the electrostatic plasma wave spectrum in the magnetosheath may be resolved into three components which may occur in any combination. Figure 1 shows spectra from three different orbits which

illustrate the three components of the spectrum. Each of the spectral measurements consists of a 5.46-min average spectrum and a 0.1-sec peak spectrum. The average spectrum taken from orbit 18 shows the first of the three components, a low frequency component which shows a generally smooth decrease in spectral density with increasing frequency. The low frequency component of the spectrum bears some resemblence in shape to the spectrum of electrostatic turbulence which occurs at the bow shock (Rodriguez and Gurnett, 1975) even though the low frequency component is usually less intense and does not extend to as high frequencies as the bow shock spectrum. The low frequency magnetosheath spectrum will be referred to as a "shock-like" spectrum of electrostatic turbulence. The peak spectrum from orbit 18 shows a shape at low frequencies similar to that of the average spectrum but also has a broad high frequency component not evident in the average spectrum. Recalling the difference between the averaging times for the peak and average spectra, it is clear that the high frequency component in the peak spectrum results from short period bursts that do not contribute significantly to the average spectrum over the long averaging period (5.46 min). Measurements of the magnetic field by the Goddard Space Flight Center magnetometer on IMP-6 determine the local electron gyrofrequency as indicated by the arrow marked f_{ge}.

The average spectrum from orbit 26 in Figure 1 illustrates the case of two components in the spectrum of electrostatic turbulence, the shock-like low frequency component similar to the case in orbit 18 and a high frequency component which peaks at the local electron plasma frequency f_{pe}. The high frequency component is identified with electron plasma oscillations and occurs at the frequency expected

for typical magnetosheath electron densities. Both peak and average spectra for the orbit 26 measurement show the feature at the electron plasma frequency, indicating that the electron plasma oscillations are present over long periods. In fact, the peak at the electron plasma frequency was observed during the entire magnetosheath traversal on orbit 26, a period of about 4 hours. From the identification of the electron plasma frequency in the spectrum, the nominal ion plasma frequency ($f_{pi} = f_{pe}/43$) is indicated by the dashed arrow. The arrow at f_{pi} is dashed to indicate that oscillations at f_{pi} are usually not considered as normal modes of a plasma due to the high damping of oscillations at the ion plasma frequency (Krall and Trivelpiece, 1973). However as will be shown below, f_{pi} may determine a lower limit on the third characteristic component of magnetosheath electrostatic waves.

The third component is illustrated by the average spectrum from orbit 37 in Figure 1. The third component is an intermediate frequency feature which appears in both peak and average spectra for orbit 37. The peak at the electron plasma frequency is also clearly evident in the peak spectrum, as is the shock-like low frequency component. In the average spectrum, the shock-like component is weak and the high frequency component almost imperceptible. In both peak and average spectra the nominal ion plasma frequency f_{pi} appears to set the low frequency limit of the intermediate frequency component.

Based on the discussion above, the three-component spectrum of magnetosheath electrostatic turbulence is indicated schematically in Figure 1, i.e., the shock-like low frequency component, the intermediate frequency component, and the high frequency component associated with

electron plasma oscillations. It is emphasized that the three spectral components are not always as clearly defined as in the three measurements in Figure 1. As may be seen from the schematic plot, the total spectrum will result from possibly independent variations in the intensities of the three components. Generally, some combination of the three components is observed, making it difficult to always clearly resolve the components. This is especially true for the intermediate frequency component, which often appears to merge with either the high or low frequency components so that the spectrum displays a broadened low or high frequency component. An example is shown in the peak spectrum from orbit 18, where instead of a peak at high frequencies which defines the electron plasma frequency, a broad high frequency feature occurs, apparently resulting from a smooth merging of short period bursts at both intermediate and high frequencies. In many cases, the components stand out more clearly in the peak spectrum than they do in the average spectrum, or, a component may appear only in the peak spectrum, examples of which are also shown in Figure 1. However, from an extensive examination of electric field spectra in the magnetosheath, the three electrostatic components schematically represented in Figure 1 are found to be the characteristic features into which the spectrum can usually be resolved.

DISTRIBUTION OF ELECTROSTATIC TURBULENCE

In order to study the electrostatic turbulence occurring throughout the magnetosheath a survey computer program was used which selects spectra that characterize the magnetosheath and discriminates against observations from other regions of plasma wave noise around the earth. The selection criterion used for the survey was developed from a study of magnetosheath spectra like those in Figure 1; the selection criterion requires that the average and peak spectra at a given observation point simultaneously exceed the corresponding threshold spectrum shown in Figure 2. The ability of the selection criterion to correctly identify magnetosheath spectra is indicated by the occurrence plot in Figure 3. In Figure 3, a cross is drawn at the radial distance and local time coordinates, rotated along the local time meridian into the ecliptic plane, of a point along the spacecraft trajectory at which the selection criterion was met. Also, the plot of Figure 3 compensates for the variation of spacecraft velocity with radial distance (and the resulting variation in spatial sampling density) so that a uniform distribution of data points occurs along the spacecraft trajectory. It may be seen that the resulting occurrence plot, in which one year of IMP-6 data is used, maps out the magnetosheath. It may also be seen that the magnetopause boundary is somewhat better defined than the bow shock, an effect which is partly related to the similarity between magnetosheath and solar wind electrostatic turbulence, and partly due to the radial movement of the bow shock in response to variations in solar wind pressure. In cases where the selection criterion was met at large radial distances,

the individual trajectories were examined to ascertain which of the above two effects might be responsible. For a few orbits, points at large radial distances (beyond about 25 R_e and for local times from about 0800 to 1500 UT) result from magnetosheath electrostatic turbulence. Such cases are due to low Mach number conditions in the solar wind which lead to unusually distant locations of the bow shock (Fairfield and Feldman, 1975). However, most of the points in the radial distance-local time region mentioned above are due to electrostatic turbulence which occurs in the solar wind. The source of such solar wind electrostatic turbulence is undoubtedly the superthermal electrons emitted into the solar wind by the bow shock. These electrons are guided along interplanetary magnetic field lines that connect the bow shock and the observing spacecraft (Fredricks et al., 1972) and tend to be detected sporadically, in part due to the changing direction of the interplanetary magnetic field, and perhaps also because of the sporadic nature of the acceleration mechanism in the bow shock. Thus, unlike the magnetosheath, solar wind electrostatic turbulence tends to be sporadic, as indicated by the isolated occurrence of crosses in the solar wind region of Figure 3. Since the threshold spectrum of Figure 2, which was determined for magnetosheath electrostatic turbulence, also corresponds to some cases of solar wind electrostatic turbulence (the solar wind turbulence indicated in Figure 3 is only a subset of the electrostatic turbulence spectra which occur in the solar wind), we have evidence of a possible similarity between the source mechanisms of magnetosheath and solar wind electrostatic turbulence. Such a possible similarity will be discussed below. Figure 3 also shows a few isolated points which met the selection

criterion in the magnetotail. The similarity between electrostatic noise in the magnetosheath and in the magnetotail has been noted by Gurnett et al. (1976).

The continuous presence of electrostatic turbulence in the magnetosheath is shown by the nearly uniform distribution of points in Figure 3. Figure 4 shows the magnetosheath boundaries obtained by drawing dashed lines through the "average" outer limits of the point distribution of Figure 3. The dashed lines obviously correspond to the average locations of the bow shock and magnetopause. The aberration angle due to the earth's orbital motion is clearly evident. Over the lifetime of IMP-6 ($\sim 3\frac{1}{2}$ yrs) three independent plots similar to Figures 3 and 4 are possible, all of which give approximately the same bow shock and magnetopause locations. Also shown in Figure 4 are portions of the inbound trajectories of orbits 18, 26, and 37, with a dot on each trajectory indicating where the spectra of Figure 1 were obtained. Orbit 15 is considered below.

The occurrence plot of Figure 3 merely maps out the spatial location of the magnetosheath. As a prelude to the study of the intensity distribution of electrostatic turbulence in the magnetosheath, a frequency

of occurrence distribution is more useful. Using the previously defined selection criterion, Figure 5 shows the frequency of occurrence of magnetosheath spectra exceeding the threshold spectrum of Figure 2. The coordinate system of Figure 5 is rectangular, in contrast to the polar coordinate system used in Figure 3, and has the effect of producing a distortion of the magnetosheath geometry of Figure 3. The bow shock and magnetopause boundaries in the rectangular system are indicated by arrows in Figure 5. The location of the solar wind is indicated on the left side of the figure; the magnetotail is divided into two regions (0 and 24 hrs local time are the same coordinate). The grid size for the distribution of Figure 5 is a square of dimensions one earth radius by one hour of local time. The frequency of occurrence in each square of the grid is calculated by dividing the number of spectra meeting the selection criterion by the number of spectra measured. The sampling is adjusted so that all squares have approximately the same number of spectral measurements. A lower limit of 1% on the acceptable frequency of occurrence has effectively removed almost all of the solar wind electrostatic turbulence. Generally, the highest frequencies of occurrence are seen to occur in the central regions of the magneto-sheath, as expected. The prominent peaks in the distribution of the frequency of occurrence are not considered significant, since in a given square, sampled points can be taken from orbits many days apart (the orbital period is about 4 days) over which time the local spectrum can surely undergo variations. Almost two years of IMP-6 data are used in the plot of Figure 5.

An intensity distribution of electrostatic spectral density at a given frequency may be obtained as a subset of the frequency of occurrence distribution by setting a lower limit of 5% on the frequency of occurrence for the intensity distribution, i.e., in any given square of the grid, the frequency of occurrence of the threshold spectrum must be at least 5% before the measurements in that square are used to calculate an average intensity. The resulting distribution of spectral densities at 1 kHz (one of the channel frequencies of the spectrum analyzer) is shown in Figure 6 for the 5.46-min average measurements. It is evident that the 5.46-min averages of spectral density are nearly uniform throughout the magnetosheath, indicating a quasi-steady state level of electrostatic turbulence of the order of 5×10^{-14} volts^2 m^{-2} Hz^{-1} at 1 kHz. Distributions similar to Figure 6 are obtained at other frequencies where the 5.46-min averages are not too near to the instrument noise level.

Figure 7 shows the intensity distribution for the 0.1-s peak measurements at 1 kHz. In this case, there is evidence that the spectral density distribution has a definite association with the bow shock. (Recall the bow shock geometry as indicated in Figure 5.) The spatial peak in the intensity distribution suggests that the electrostatic turbulence generated at the bow shock persists for a substantial distance into the magnetosheath, especially in the subsolar region. The intensity of electrostatic turbulence also appears to decrease with distance from the bow shock more quickly in the dusk region than in the dawn region. The apparent spatial dependence of Figure 7 is also reproduced for peak measurements at other frequencies near 1 kHz. From previous discussion it may be recalled that the low frequency

shock-like component of magnetosheath electrostatic turbulence occurs in the vicinity of 1 kHz. Thus, Figure 7 illustrates the association of magnetosheath low frequency electrostatic turbulence with the bow shock, hence the previous reference to this component as shock-like. The intermediate frequency component of magnetosheath electrostatic turbulence, the less well-defined of the three characteristic components, cannot be clearly resolved in an intensity distribution plot like Figure 7, where averaging tends to smooth out the gentle peaks of individual spectra. However, since the intermediate frequency component often is indistinguishable from a broad low frequency component, the bow shock dependence indicated in Figure 7 may also be an relation displayed by the intermediate frequency component.

At the higher frequency of the third component of the magnetosheath plasma wave spectrum, the distribution of electrostatic turbulence is indicated by Figure 8, where the peak spectral density measurements at 56.2 kHz are used. (The 5.46-min averages at high frequencies are too often near the noise level to allow an accurate intensity distribution to be determined.) The high frequency component is associated with the electron plasma frequency, which for typical magnetosheath electron densities occurs in the range 30-60 kHz. The distribution of peak intensities at 56.2 kHz shows that the noise distribution has a maximum in the subsolar region of the magnetosheath, but without any apparent association with the bow shock as for the low frequency component. Toward the dawn and dusk regions the intensity distribution drops off, suggestive of the electron density variation expected on the basis of model calculations (Spreiter et al., 1966). Thus as the electron density

decreases due to the increasing magnetosheath flow velocity, the intensity at 56.2 kHz corresponds to a measurement somewhere on the high frequency side of a spectral density peak at the local plasma frequency.

The spectral density distributions for the frequencies used in Figures 6, 7 and 8 are shown in Figure 9. It may be seen that at 1 kHz both the peak and average measurements exhibit Gaussian-like distributions in the logrithm of the spectral density. The means of the spectral densities are indicated by a dot and the error bars are at one standard deviation, i.e., $< E^2(f) > \pm \sigma$, where $E^2(f)$ is the spectral density, and the brackets indicate a mean value. The step size in the spectral density intervals used in the intensity distribution plots of Figure 6, 7 and 8 are approximately equivalent to $< \sigma >$. Table 1 lists the spectral density means and standard deviations of magnetosheath electrostatic turbulence for the frequency range 20 Hz - 70 kHz, corresponding to the first 14 channels of the spectrum analyzer. The mean values are based on the 0.1-s peak measurements.

VARIATION OF MAGNETOSHEATH ELECTROSTATIC TURBULENCE

The effect of a change in the thermodynamic state of the magnetosheath plasma on the spectrum of electrostatic turbulence is of interest since such an effect can provide a clue to the source mechanism of electrostatic turbulence. Figure 10 shows a clear example of a change in state of the subsolar magnetosheath during the inbound trajectory of orbit 15. The upper panels show eight of the sixteen channels of the electric field spectrum analyzer measurements, with peaks plotted as dots and averages as vertical lines. The eight channels cover the frequency range 1.0-56.2 kHz. The electric field measurements show that the bow shock is encountered at about 1603 UT when the sudden jump in field intensity above the solar wind level occurs. Following the shock crossing, there is an enhanced level of electrostatic noise, less intense than at the shock but still above the levels detected in the solar wind just before the shock crossing. The enhanced electrostatic turbulence at times after about 1605 UT is typical of magnetosheath electric field observations. The lower panel of Figure 10 is a plot of $|\vec{B}|$, the magnetometer measurement of the magnitude of the magnetic field during the same magnetosheath traversal. The orientation of the magnetic field vector is given by φ_B and θ_B, the solar ecliptic longitude and latitude, respectively. It can be seen that upon entering the magnetosheath, the magnetic field vector maintains an average direction approximately perpendicular to the ecliptic plane. The magnetic field vector is also approximately perpendicular to the shock normal determined by the model of Fairfield (1974), and therefore the bow shock is approximately

a perpendicular shock. Fluctuations in the magnetosheath magnetic field intensity are clearly evident in contrast to the relatively steady magnetic field in the solar wind. At about 1700 UT the magnetic field vector rotates through about 90^{o} so that the vector now lies approximately in the ecliptic plane ($\theta_B \sim 0^{o}$). Close to the same time, the IMP-5 spacecraft, which was in the solar wind near the bow shock at a local time of about 15 hr, recorded a similar rotation of the magnetic field vector (D. H. Fairfield, private communication, 1976), thus indicating that it was interplanetary discontinuity that convected past the IMP-6 spacecraft at 1700 UT. The new orientation of the magnetosheath magnetic field is retained until the magnetopause encounter at about 1805 UT. Since an interplanetary discontinuity generally separates two different thermodynamic states of the solar wind plasma (Burlaga, 1971), the magnetosheath state in the interval 1605-1700 UT is probably different from that in the interval 1700-1800 UT. The effect of such a change in state on the spectrum of electrostatic turbulence is most evident in the high frequency channels of the upper panel in Figure 10, where it can be seen that at 1700 UT the electric field intensity increases by about an order of magnitude and remains at the new level until the magnetopause is reached. Other interplanetary discontinuities which have been detected in the solar wind do not exhibit the increase of electrostatic turbulence at higher frequencies shown in Figure 10; therefore, we may conclude that the difference in states across the discontinuity is probably enhanced by interaction with the bow shock. Points A and B refer to times before and just after the interplanetary discontinuity was detected, and point C refers to a time just

before the magnetopause is crossed. The points along the spacecraft trajectory on orbit 15 corresponding to A, B, and C are indicated in Figure 4. The spectra of electrostatic turbulence at points A, B, and C are shown in Figure 11. The spectra are plotted in a format similar to that of Figure 1 and may be compared to those spectra. Spectrum A shows that the shock-like low frequency component is clearly evident in the average spectrum with a weak high frequency component in the vicinity of the expected electron plasma frequency f_{pe}. The nominal ion plasma frequency determined from $f_{pi} = f_{pe}/43$ and the electron gyrofrequency f_{ge} computed from the measured magnetic field are also indicated. The peak spectrum shows a much broader high frequency component and is apparently a case of the intermediate component merging with the high frequency component. The spectra in panel B occur just after the discontinuity passes the spacecraft and it may be seen that an intense burst of electron plasma oscillations is detected in the peak spectrum. The value of f_{pe} does not appear to have changed greatly between panels A and B, although frequency resolution is limited to a change which corresponds to an electron density change by about a factor of two. Thus it is likely that the peak at f_{pe} in panel B does not arise from a frequency shift toward higher frequencies due to a large increase in electron density across the discontinuity. Instead, it is likely that the electron distribution function has changed substantially in the plasma behind the discontinuity, possibly involving beam-plasma or drift instabilities which are more conducive to the generation of high frequency electrostatic turbulence. The average spectrum in panel B shows that the intermediate frequency component, corresponding to the range $f_{pi} < f < f_{pe}$, has also been enhanced and becomes better resolved from both the low and high frequency components. The state

change across the discontinuity appears to have had little effect on the low frequency component, corresponding to the range $f \lesssim f_{pi}$. The spectra in panel C show that the changed state of the magnetosheath plasma maintains approximately the same electrostatic spectrum up to the time near the magnetopause crossing, with all three characteristic components of electrostatic turbulence fairly well resolved. Data profiles similar to that of Figure 10, which imply sudden changes in state for the magnetosheath, have occurred on several other orbits. These cases were also probably caused by interplanetary discontinuities.

WAVELENGTH ESTIMATES

The plasma wave spectra discussed above were measured in a streaming plasma; thus, if a Doppler shift in the spectrum can be observed, an estimate of the wavelength of the plasma waves can be obtained. From the Doppler formula $2\pi f = 2\pi f_o + \vec{k}\cdot\vec{V}_{ms}$, where f is the observed frequency, f_o is the unshifted frequency, $|\vec{k}| = 2\pi/\lambda$ is the wave number corresponding to wavelength λ, and $\vec{V}_{ms}$ is the magnetosheath flow velocity, the maximum Doppler shift is $\Delta f_D = f - f_o = V_{ms}/\lambda$. In a broad region over the subsolar magnetosheath, a typical flow velocity is $V_{ms} \sim 200$ km sec^{-1}.

For electron plasma waves, identified with the high frequency component, to be weakly damped the wave phase velocity v_p must satisfy the relation $v_p = f\lambda \gg v_{th}$, where v_{th} is the electron thermal speed. A typical value for v_{th} in the magnetosheath is $\sim 10^3$ km sec^{-1}. Thus, if we take $v_p \sim$ (10-100) $v_{th} = (10^4\text{-}10^5)$ km sec^{-1} and $f \sim 50$ kHz, the wavelength of electron plasma waves is $\lambda \sim$ (0.2-2) km. The corresponding Doppler shift is $\Delta f_D \sim$ (1-0.1) kHz, which is within the bandwidth of

the high frequency channel filters (bandwidth $\sim$ 10% or about 3-6 kHz). Therefore, consistent with observations, detectable Doppler shifts are not expected for electron plasma waves, and the spectral peak at f_{pe} is a well defined normal mode of oscillation with a wavelength on the order of one kilometer. Frequency shifts that do occur are undoubtedly caused by a change in plasma density. The model calculations of Spreiter et al. (1966) indicate that a maximum density change by a factor of about 4 can occur in the magnetosheath, corresponding to a change in the electron plasma frequency by a factor of 2. Such changes in plasma frequency are consistent with the spectral peaks observed in the 31.1 kHz and 56.2 kHz channel frequencies.

At lower frequencies the wavelengths are difficult to estimate since the normal modes of oscillation are uncertain. Doppler shifted ion acoustic waves might correspond to the observed lower frequencies except that for the magnetosheath plasma the electron to proton temperature ratio is $Te/Tp \leqslant 1$, a situation for which ion acoustic waves are highly damped (unlike the case at the bow shock, where electron preheating in the initial part of the magnetic field gradient of the shock can make $Te/Tp > 1$, resulting in undamped ion acoustic waves (Rodriguez and Gurnett, 1976)). If we take the minimum possible wavelength to be the Debye length λ_{De} ($\sim$ 20 m for the magnetosheath), then the maximum Doppler shift expected is Δf_D = 200 km sec^{-1}/20 m = 10 kHz. We can look for evidence of such Doppler shifts by examining the spectra measured during traversals of the subsolar magnetosheath that pass through the expected location of the stagnation point for magnetosheath flow, i.e., the subsolar magnetopause (Alksne, 1967). During such a

traversal the typical magnetosheath flow velocity will change from $V_{ms} \sim 200$ km sec^{-1} immediately behind the bow shock to $V_{ms} \sim 0$ near the magnetopause, and if $\lambda \sim \lambda_{De}$, a maximum frequency shift of $\Delta f_D \sim \Delta V/\lambda_{De} \sim 10$ kHz would occur in the low frequency part of the magnetosheath spectrum. In the first year about four or five orbits passed through the stagnation region (orbit 15 in Figure 4 and 11 is one of these) and it is thus possible to compare magnetosheath spectra taken near the bow shock to spectra taken near the magnetopause stagnation region, for evidence of Doppler shifts. An examination of orbits passing through the stagnation region shows that, taking account of intensity variations, frequency shifts of 10 kHz are not observed; at most, 1 kHz Doppler shifts may occur. If we take 1 kHz as the maximum observable frequency shift, the minimum wavelength of the low frequency oscillations is $\lambda \sim 10\ \lambda_{De} \sim 200$ m.

The spectra from orbit 15 (Figure 11) are an especially interesting case in which to look for Doppler shifts because of the encounter with an interplanetary tangential discontinuity convected by the solar wind. Across a tangential discontinuity in the solar wind, the normal component of flow velocity $\vec{V}\cdot\hat{n}$ is conserved but the parallel component $\vec{V}\times\hat{n}$ can change, where $\vec{V}$ is the velocity vector and $\hat{n}$ is the discontinuity normal vector (Burlaga, 1971). However, once inside the magnetosheath, the velocity must conform to the flow geometry of the magnetosheath, so that $\vec{V}_t \to 0$ at the stagnation point. Therefore we may assume that in the sequence of spectra in Figure 11, the magnetosheath flow is decreasing from spectrum A to spectrum C in a uniform manner. If a large Doppler shift were present, the shift between spectra A and C should be toward lower frequencies and an apparent enhancement of intensity at low frequencies

would occur. Such a frequency shift is clearly not evident in Figure 11. In fact, the opposite occurs: the low frequency component in the average spectrum decreases in intensity, consistent with the survey results of Figure 7. Considering the intermediate frequency component which is associated with the change in plasma thermodynamic state across the discontinuity, it is clear that this component cannot be a Doppler shifted high frequency component since both components maintain distinct identities between spectra B and C. A careful examination of the intermediate frequency component in Figure 11 indicates that for this component alone, there is a slight shift of about 1 kHz toward lower frequencies between spectra B and C, as would be expected for a decreasing flow velocity. Thus, it is concluded that the low and intermediate components of electrostatic turbulence are distinct, with minimum wavelengths on the order of several hundred meters.

ELECTROSTATIC WAVES IN CURRENT SHEETS

The magnetosheath crossing of Figure 10 provides two examples of current sheets other than the bow shock, implied by gradients in magnetic field magnitude and direction, viz., the magnetopause and the interplanetary discontinuity. Associated with both the magnetopause and the discontinuity there are distinct "spikes" in electrostatic turbulence best indicated for channel frequencies below 16.5 kHz, i.e., below the electron plasma frequency. At the magnetopause, at least three spikes of electrostatic noise may be seen (in the 5.12-s average measurements, plotted as vertical bars); each spike is clearly

correlated with the gradients in the magnetic field magnitude oscillation that occurs at the magnetopause. The electrostatic spikes at the magnetopause may be similar to the intermediate frequency electrostatic turbulence in the magnetosheath, in which case the association of the spikes with currents which result from particle drifts in a magnetic field gradient provides additional information on the possible source mechanism of magnetosheath electrostatic turbulence. Adjacent to the magnetopause and within the magnetosphere, several spikes of electrostatic noise may be seen in the 31.1 kHz channel. These are probably electron plasma oscillations associated with high energy electrons trapped in the magnetosphere and undergoing wave-particle interactions with the thermal plasma just inside the magnetopause. The association of the electron plasma oscillations with the magnetopause, if any, is unclear.

ELECTRIC FIELD POLARIZATION

It is of interest to determine the electric field polarization with respect to the magnetic field direction because such information is of importance in identifying the wave modes involved in magnetosheath electrostatic turbulence. A technique was described by Rodriguez and Gurnett (1976) for determining the electric field polarization at high frequencies which resolved the spin modulation of the ambient noise. Such a technique requires that the magnetic field direction lie in the spin plane of the electric antennas, which in the case of IMP-6 coincided with the ecliptic plane, and maintain its direction relatively fixed for the period of the rapid-sample measurements. The rapid-sample measurements are 128 successive samples of a given spectrum analyzer channel, with

a time constant of 0.32 sec. About 4½ revolutions of the spacecraft occur during the sampling period. During the magnetosheath traversal of orbit 15, shown in Figure 10, the 31.1 kHz channel was rapid-sampled soon after the interplanetary discontinuity passed and the magnetic field vector provided the necessary conditions for determining the electric field polarization at 31.1 kHz. Figure 12 shows the ecliptic plane angular distribution of the rapid-sampled points. By considering each point as a unit mass particle with a moment arm equal to its fluctuation magnitude, we may calculate the principal axes of the moments of inertia in the two-dimensional distribution of rapid-sampled point. The minor principal axis has an orientation indicated by φ_p and represents the average direction of the electric field fluctuations. The solar ecliptic longitude of the magnetic field vector is given by φ_B. The difference $\varphi_B - \varphi_p$ is small enough so that it is evident that the electric field is polarized along the magnetic field direction. The polarization thus determined supports the identification of the high frequency electrostatic turbulence as electron plasma oscillations. In a previous report (Rodriguez and Gurnett, 1975) a similar determination showed that the magentosheath

electrostatic field at 3.11 kHz is also polarized along the magnetic field direction.

At lower frequencies, a different technique for determining the electric field polarization is possible which gives a finer time scale resolution by use of the wideband waveform measurement available in the range 0-1 kHz. For this technique the two orthogonal electric antennas lying in the spin plane of IMP-6 are simultaneously used in the waveform measurement and the magnetic field vector must again lie in the spin plane. The geometry depicted in Figure 13 illustrates the use of this technique for polarization measurement. In the spacecraft frame of reference, the magnetic field vector is seen rotating clockwise through the four quadrants defined by the two electric antennas, signified by E_x and E_y. The angle $\varphi(B, Ey)$ defines the rotation phase angle of the magnetic field vector, passing through 360° for one revolution of the spacecraft. Generally, the electric field can be polarized either parallel or perpendicular to the magnetic field direction, as indicated by $E_{\parallel}$ and $E_{\perp}$. As the magnetic field vector rotates (in the spacecraft frame) the polarity of the detected waveform will change due to the antenna polarities. The correlation of the waveforms detected by the two electric antennas will have particular algebraic signs associated with $\varphi(B, Ey)$, depending on whether the electric field is polarized parallel or perpendicular to the magnetic field.

Thus quadrant 1 has a + sign because the product $(+E_x)$ $(+E_y)$ is positive, and quadrant 2 has a - sign because the product $(+E_x)$ $(-E_y)$

is negative. Therefore, if E $\parallel$ B, then for $0^{o} < \varphi(B, Ey) < 90^{o}$ and $180^{o} < \varphi(B, Ey) < 270^{o}$ (quadrants 1 and 3) the correlation of E_x and E_y is positive, and for $90^{o} < \varphi(B, Ey) < 180^{o}$ and $270^{o} < \varphi(B, Ey) < 360^{o}$ (quadrants 2 and 4) the correlation of E_x and E_y is negative. If E $\perp$ B, the signs of the four quadrants are reversed from the case for E $\parallel$ B. Thus, by noting the value of $\varphi(B, E_y)$ in conjunction with the correlation of E_x and E_y we may determine which of the above cases occurs, E $\parallel$ B or E $\perp$ B.

The correlation of E_x and E_y for the frequency range 0-1 kHz in the magnetosheath is shown in Figure 14, for a magnetosheath interval from orbit 263. The central panel shows both the positively and negatively correlated signals of the waveform measurement. The upper panel shows the magnetic field magnitude $|\vec{B}|$ and the solar ecliptic longitude and latitude, φ_B and θ_B. The correlation technique requires that $\theta_B \sim 0^{o}$ and the plot of θ_B shows that this condition is sufficiently well met for the time interval displayed. It is also advantageous that φ_B remain steady since the angle $\varphi(B, Ey) = \varphi_B - \varphi_{E_y}$, where φ_{E_y} is the azimuthal angle of the E_y antenna from the solar direction, then varies smoothly through 360^{o} as the spacecraft rotates. The lower panel is a plot of the phase of $\varphi(B, E_y)$ as a function of time. From the lower panel, we may demarcate the ranges 0^{o} - 90^{o}, 90^{o} - 180^{o}, 180^{o} - 270^{o}, and 270^{o} - 360^{o}, and by reference to the correlation results in the central panel, determine the algebraic sign of the correlation in the corresponding quadrant. Thus, beginning at about 0122:05 UT, the correlation is positive for the range 0^{o} - 90^{o}, negative for the range 90^{o} - 180^{o}, etc. The sequence of correlation signs is maintained throughout the entire interval of

about 2½ minutes. Referring to Figure 13, it can be seen that the sequence of correlation signs in Figure 14 corresponds to E ∥ B. Therefore, magnetosheath electrostatic plasma waves in the range 0-1 kHz are polarized along the magnetic field direction, similar to the result obtained for higher frequency electrostatic turbulence.

It is of interest to apply the same correlation technique to waveform measurements obtained in the bow shock, since in a previous report (Rodriguez and Gurnett, 1975) only an incomplete measurement using the rapid-sample technique was available. Figure 15 shows the waveform correlation that results at the bow shock crossing that occurred about two minutes before the magnetosheath data of Figure 14. In Figure 15, the shock transition occurs in the interval 0120:10 - 0120:30 UT, with the downstream magnetosheath after 0120:30 UT. The requirement that $\theta_B \sim 0^o$ is less well met in the bow shock region so that the waveform correlation in the central panel of Figure 15 is correspondingly less well defined. However, if we first determine the electric field polarization in the downstream magnetosheath (at about 0120:42 - 0120:55 UT), and then project the resulting sequence of sign reversals into the bow shock region, we can check for consistency of the inferred polarization. The downstream magnetosheath polarization again corresponds to E ∥ B. It may be seen that in the interval 0120:17 - 0120:21 UT where the values of θ_B and φ_B are momentarily steady, the inferred quadrant sign and the waveform correlation both have a negative sign. Thus, the data of Figure 15 are consistent with the previous conclusion that the fluctuation electric field in the bow shock is polarized along the magnetic field direction.

SUMMARY OF RESULTS AND CONCLUSIONS

The typical spectrum of magnetosheath electrostatic plasma wave turbulence results from a combination of three characteristic components. The low frequency shock-like component, usually in the frequency range $f < f_{pi}$, is always present near the bow shock and decreases in intensity as the magnetopause is approached. Since the low frequency component resembles the bow shock spectrum, which has been associated with ion heating at the shock (Rodriguez and Gurnett, 1976), it is likely that for substantial distances into the magnetosheath, the ion temperature either remains high, comparable to the value at the shock, or perhaps continues to increase if ion-ion streaming instabilities are present. The magnetic field gradients typically observed in the magnetosheath (Fairfield, 1976) may provide the necessary currents for ion-ion streaming. The intensity of the low frequency component is usually about an order of magnitude less than the intensity of the corresponding frequencies at the bow shock; however, often the intensities are comparable so that a significant range of wave-particle interactions in the magnetosheath is most probable. Observations of both high energy protons (West and Buck, 1976) and thermal electrons and ions (Montgomery et al.,1970; Scudder et al., 1973) show that wave-particle interactions which would lead to heating and acceleration are likely.

The high frequency component of the magnetosheath spectrum peaks at the local electron plasma frequency f_{pe} and is often a well resolved feature. The maximum intensities of magnetosheath electron plasma oscillations occur in the subsolar magnetosheath where the plasma probably undergoes its greatest dynamic interactions such as deceleration, heating,

and flow deflection. The time scales of the measurements indicate that magnetosheath electron plasma oscillations are characteristically short period bursts rather than a continuous noise, although the latter case also occurs. Burst magnitudes of electron plasma oscillations are of the order of 0.1 millivolt m^{-1}. In some cases, up to 1.0 millivolt m^{-1} field strengths have occurred.

The intermediate frequency component is less well resolved than the other two components because it occurs in the frequency range $f_{pi} < f < f_{pe}$. However, it can be detected sufficiently often to be regarded as a distinct component. The intermediate frequency component suggests that there is a similarity between magnetosheath and solar wind electrostatic turbulence since electrostatic noise in the range $f_{pi} < f < f_{pe}$ is often detected in the solar wind away from the earth's influence (Gurnett and Anderson, 1977) and in the upstream region near the earth. Superthermal electron fluxes emitted from the bow shock probably generate, through beam-plasma interactions, the electrostatic turbulence detected in the solar wind near the earth. Thus a similar mechanism may be responsible for magnetosheath electrostatic turbulence, either through bow shock emission of superthermal electrons into the magnetosheath and/or generation of superthermal electrons within the magnetosheath. It may be noted that when the intermediate frequency component is resolved, as in Figures 1 and 11, the maximum intensity tends to occur at a frequency of about 2 f_{pi}. The Buneman instability has its largest growth rate near 2 f_{pi} (Fredricks et al., 1970; Hamberger and Jancarik, 1972), which corresponds to the normal mode of oscillation for quasi-particles of effective mass $\tilde{m} = (m_e/m_i)^{1/3} m_i$, where m_e is

the electron mass and m_i is the proton mass (Ionson, 1977). However, the Buneman instability requires that the electrons have a drift velocity v_{De} with respect to the protons such that $v_{De} > v_{Te}$, where v_{Te} is the electron thermal speed. The observed particle distributions in the magnetosheath have not received enough study to indicate whether such drift velocities are possible.

For all three characteristic components of magnetosheath electrostatic turbulence the electric field polarization is parallel to the local magnetic field direction $E \parallel B$. This electric field polarization implies that the wave vector is also parallel to the magnetic field, $k \parallel B$. Electrostatic plasma wave modes with $k \parallel B$ are of the longitudinal kind, electron plasma oscillations and ion sound waves, and these are likely the wave modes which are involved in magnetosheath electrostatic turbulence.

TABLE 1. Mean Magnetosheath Spectrum (0.1-s)

Ch1	Frequency	Spectral Density (volts^2 m^{-2} Hz^{-1}) Mean	Mean +σ	Mean -σ
0	36 (Hz)	5.2 E-09	2.3 E-08	1.2 E-09
1	63	2.0 E-09	8.5 E-09	4.8 E-10
2	120	1.2 E-09	4.4 E-09	3.0 E-10
3	200	2.8 E-10	1.6 E-09	4.8 E-11
4	311	2.0 E-10	2.1 E-09	2.0 E-11
5	562	1.0 E-10	1.7 E-09	6.0 E-12
6	1.00 (kHz)	7.6 E-11	2.0 E-09	2.9 E-12
7	1.78	2.4 E-11	9.0 E-10	6.6 E-13
8	3.11	2.6 E-12	9.3 E-11	7.4 E-14
9	5.62	1.8 E-13	3.7 E-12	9.0 E-15
10	10.62	3.3 E-14	4.6 E-13	2.3 E-15
11	16.5	7.4 E-15	1.0 E-13	5.4 E-16
12	31.1	4.7 E-15	1.2 E-13	1.9 E-16
13	56.2	5.9 E-16	1.1 E-14	3.2 E-17

σ = Logrithmic Standard Deviation

ACKNOWLEDGEMENTS

I wish to thank several people who have helped considerably to make this study possible: D. Gurnett, A. Lang, and J. Green at the University of Iowa; thanks are also due to my colleagues at Goddard Space Flight Center whose suggestions and support are appreciated: D. Fairfield, J. Alexander, M. Kaiser, and M. Goldstein. Invaluable data processing assistance was provided by D. Howell, F. Ottens, and R. Thompson.

REFERENCES

Alksne, A.Y., The steady-state magnetic field in the transition region between the magnetosphere and the bow shock, Planet. Space Sci., 15, 239, 1967

Burlaga, L.F., Hydromagnetic waves and discontinuities in the solar wind, Space Sci. Rev., 12, 600, 1971.

Fairfield, D. H., Whistler waves observed upstream from collisionless shocks, J. Geophys. Res., 79, 1368, 1974.

Fairfield, D. H., Magnetic fields of the magnetosheath, Rev. Geophys. Space Phys., 14, 117, 1976.

Fairfield, D. H., and W.C. Feldman, Standing waves at low Mach number laminar bow shocks, J. Geophys. Res., 80, 515, 1975.

Fredricks, R.W., G.M. Crook, C.F. Kennel, I.M. Green, and F.L. Scarf, OGO 5 observations of electrostatic turbulence in bow shock magnetic structures, J. Geophys. Res., 75, 3751, 1970.

Fredricks, R.W., F.L. Scarf, and I.M. Green, Distributions of electron plasma oscillations upstream from the earth's bow shock, J. Geophys. Res., 77, 1300, 1972.

Gurnett, D.A., and R.R. Anderson, Plasma wave electric fields in the solar wind: Initial results from Helios-1, J. Geophys. Res., 82, 632, 1977.

Gurnett, D.A., L.A. Frank, and R.P. Lepping, Plasma waves in the distant magnetotail, J. Geophys. Res., 81, 6059, 1976.

Hamberger, S.M., and J. Jancarik, Experimental studies of electrostatic fluctuations in a turbulently heated plasma, Phys. Fluids, 15, 825, 1972.

Ionson, J.A., Nonlinear saturation of the Buneman instability, Phys. Lett. 60A, 1, 27, 1977.

Krall, N.A., and A.W. Trivelpiece, Principles of Plasma Physics, McGraw-Hill Book Company, New York, 1973.

Montgomery, M.D., J. R. Asbridge, and S.J. Bame, Vela 4 plasma observations near the earth's bow shock, J. Geophys. Res., 75, 1217, 1970.

Rodriguez, P. and D.A. Gurnett, Electrostatic and electromagnetic turbulence associated with the earth's bow shock, J. Geophys. Res., 80, 19, 1975.

Rodriguez, P. and D.A. Gurnett, Correlation of bow shock plasma wave turbulence with solar wind parameters, J. Geophys. Res., 81, 2871, 1976.

Scarf, F.L., R.W. Fredricks, L.A. Frank, and M. Neugebauer, Nonthermal electrons and high-frequency waves in the upstream solar wind, 1. Observations, J. Geophys. Res., 76, 5162, 1971.

Scudder, J. D., D.L. Lind, and K.W. Ogilvie, Electron Observations in the solar wind and magnetosheath, J. Geophys. Res., 78, 6535, 1973.

Smith, E.J., and B.T. Tsurutani, Magnetosheath lion roars, J. Geophys. Res., 81, 2261, 1976.

Spreiter, J.R., A. L. Summers, and A. Y. Alksne, Hydromagnetic flow around the magnetosphere, Planet. Space Sci., 14, 223, 1966.

West, H.I., Jr., and R.M. Buck, Observations of >100-Kev protons in the earth's magnetosheath, J. Geophys. Res., 81, 569, 1976.

FIGURE CAPTIONS

Figure 1. Sample measurements of the magnetosheath spectrum of electrostatic turbulence in the frequency range 20 Hz to 200 kHz. The three characteristic spectral components inferred are shown schematically in the lower right hand panel. Average spectra (AV) are 5.46-min averages and peak spectra (PK) are 0.1-s averages. The electron plasma frequency f_{pe} is determined from the presence of a narrow band high frequency maximum, the nominal ion plasma frequency $f_{pi} = f_{pe}/43$, and the electron gyrofrequency f_{ge} is calculated from the measured magnetic field.

Figure 2. The threshold spectrum for the peak and average measurements which identifies magnetosheath electrostatic turbulence.

Figure 3. The occurrence plot for peak and average spectral density measurements which exceed the threshold spectrum of Figure 2. The testing of spectral measurements against the threshold spectrum is adjusted to produce a uniform spatial sampling density along the spacecraft trajectory. Plotted points are rotated in a local time meridian plane into the ecliptic plane. The plotted points clearly map out the magnetosheath.

Figure 4. Average magnetosheath boundaries (corresponding to the bow shock and magnetopause) based upon the occurrence plot of Figure 3. Note the aberration in both the bow shock and magnetopause caused by the earth's orbital velocity. Portions of the inbound trajectories (which lie approximately in the ecliptic plane) of orbits 15, 18, 26, and 37 are indicated. The short bars crossing the trajectories indicate the locations of bow shock and magnetopause crossings on those particular orbits.

Figure 5. The frequency of occurrence of magnetosheath electrostatic turbulence satisfying the threshold spectrum of Figure 2. The rectangular coordinate system is equivalent to the polar plot of Figure 3. The normal geometry of the magnetosheath is distorted in the rectangular plot so that the bow shock and magnetopause are as indicated. About two years of IMP-6 data were used to provide approximately uniform normalization. The central region of the magnetosheath corresponds to the highest frequencies of occurrence.

Figure 6. The magnetosheath spectral density distribution at 1 kHz for the 5.46-min average measurements. The quasi-steady state nature of magnetosheath electrostatic turbulence is evident in the almost uniform level of intensity as defined by the spectral density levels SD2 and SD3.

Figure 7. The spectral density distribution at 1 kHz for the 0.1-s peak measurements. The association of low frequency electrostatic turbulence with the bow shock is indicated by the almost monotomic decrease over about two decades of spectral density with distance from the bow shock.

Figure 8. The distribution of magnetosheath spectral densities for electron plasma oscillations at 56.2 kHz based on the 0.1-s peak measurements. The highest level of electron plasma oscillations occurs in the subsolar region of the magentosheath, without apparent association to the bow shock. The intensity drops off toward both the dawn and dusk regions, suggestive of the decrease in electron number density.

Figure 9. The distribution of magnetosheath spectral density measurements at 1.0 and 56.2 kHz corresponding to the intensity distributions of Figures 6, 7, and 8. The dot and error bars indicate the mean and standard deviations of the distributions.

Figure 10. Traversal of the subsolar magnetosheath on orbit 15 inbound. The upper panels show 8 channels of electric field peak (dots) and average (bars) measurements for the frequency range 1.0-56.2 kHz. The lower panels show the magnetic field magnitude and direction angles. The bow shock is crossed at 1603 UT, an interplanetary discontinuity is detected at 1700 UT where the magnetic field vector rotates into the ecliptic plane ($\theta_B \rightarrow 0^o$), and the magnetopause (approximately the stagnation region) is crossed at about 1805 UT. Intense electron plasma oscillations are detected upstream of the bow shock (before 1603 UT) and in the magnetosheath after passage of the discontinuity. The appearance of an enhanced intermediate frequency component is evident after 1700 UT in the peak and average measurements from 3.11 kHz to 31.1 kHz. A rapid-sample measurement of the 31.1 kHz channel occurs over the interval indicated. The spacecraft trajectory for the period above is shown in Figure 4. At times indicated by A, B, and C, the spectra of Figure 11 were measured.

Figure 11. Magnetosheath spectra corresponding to time indicated by A, B, and C in Figure 10. Spectrum A is the magnetosheath spectrum before the interplanetary discontinuity is detected and shows the low frequency ($f < f_{pi}$) and high frequency ($f \sim f_{pe}$) components. Spectra B and C occur after passage of the discontinuity and illustrate the enhancement of the intermediate frequency ($f_{pi} < f < f_{pe}$) component

in the new thermodynamic state of the magnetosheath. The peak at f_{pe} in spectrum B corresponds to an electric field of ~ 1 millivolt m^{-1}. Spectrum C occurs near the magnetopause in the region of stagnation for magnetosheath flow. Spectra A and B may be compared to spectrum C for evidence of Doppler shifts in frequency.

Figure 12. A polar plot of rapid-sample measurements versus spacecraft spin angle for the enhanced magnetosheath turbulence at 31.1 kHz in Figure 10. The minor principal axis φ_p of the azimuthal point distribution indicates that that electrostatic oscillations are polarized along the magnetic field direction φ_B.

Figure 13. Schematic diagram of IMP-6 antennas and spacecraft rotation which illustrates the waveform correlation technique. The angle between $\vec{B}$ and the positive polarity end of the E_y antenna is $\varphi(B, E_y)$. The phase of $\varphi(B, E_y)$ passes through 360^o for one rotation of the spacecraft. $E_{\parallel}$ and $E_{\perp}$ are possible polarizations of the electric field which the waveform correlation seeks to establish. Quadrants 1, 2, 3, and 4 are defined as indicated.

Figure 14. The waveform correlation for magnetosheath electrostatic turbulence in the range 0-1 kHz is shown in the central panel, with the negatively and positively correlated signals separated. Magnetic field measurements are shown in the upper panel. The phase angle $\varphi(B, Ey)$ is shown in the lower panel for about 6 spacecraft rotations. The correlation sign which corresponds to a given quadrant is determined as indicated in the time interval 0122:04 - 0122:17 UT. The sign sequence is indicated above the phase angle plot and corresponds to $\vec{E} \parallel \vec{B}$.

Figure 15. The waveform correlation for the bow shock region. The bow shock transition occurs in the time interval 0120:10 - 0120:30 UT. The correlation signs through the transition region appear to be consistent with the sequence determined in the downstream region (after 0120:30 UT) which give $\vec{E} \parallel \vec{B}$.

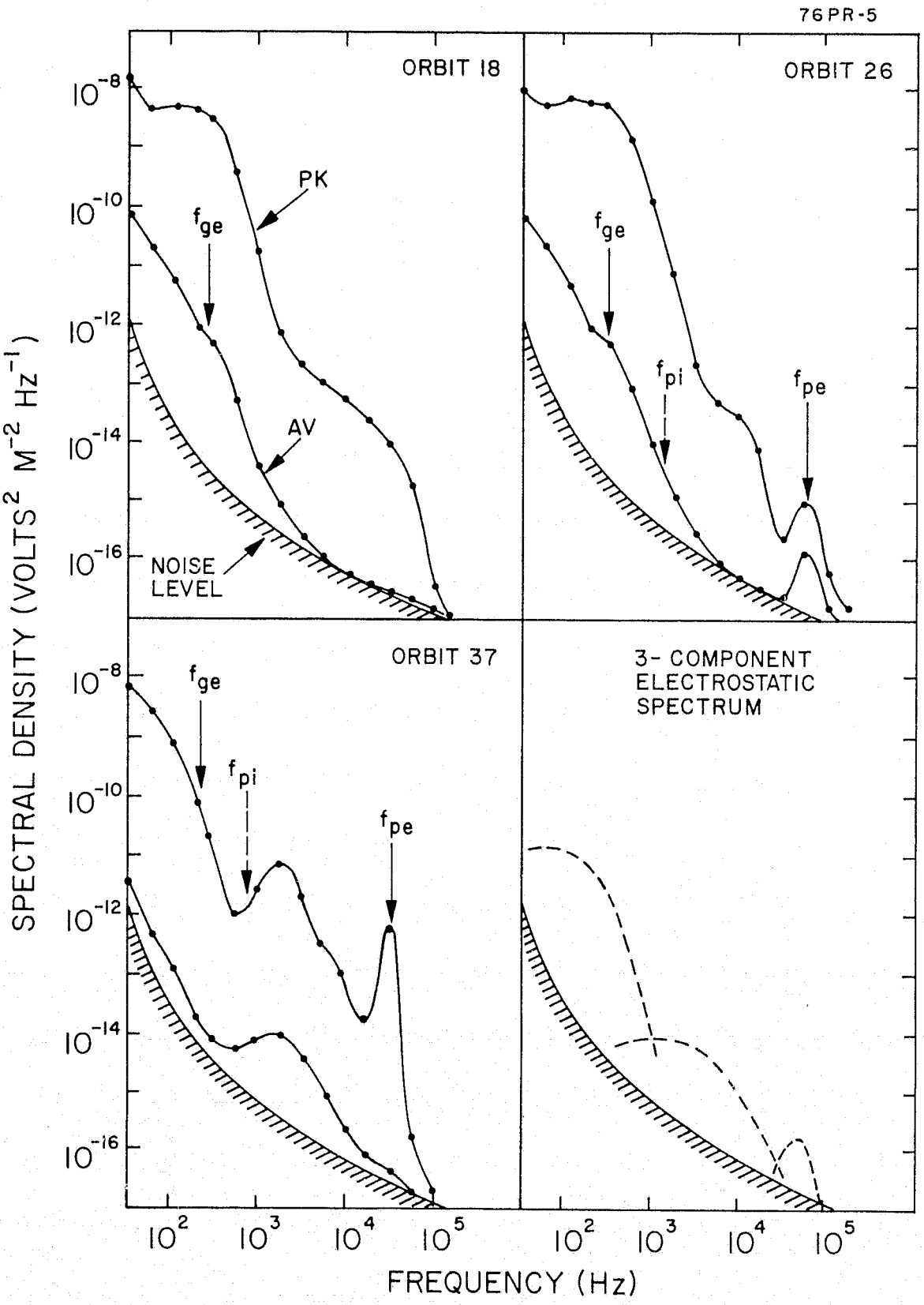
76PR-5
ORBIT 18
ORBIT 26
ORBIT 37
3- COMPONENT
ELECTROSTATIC
SPECTRUM
PK
AV
NOISE
LEVEL
f_{ge}
f_{pi}
f_{pe}
SPECTRAL DENSITY (VOLTS^2 M^{-2} Hz^{-1})
FREQUENCY (Hz)
10^{-8}
10^{-10}
10^{-12}
10^{-14}
10^{-16}
10^2
10^3
10^4
10^5

Figure 1

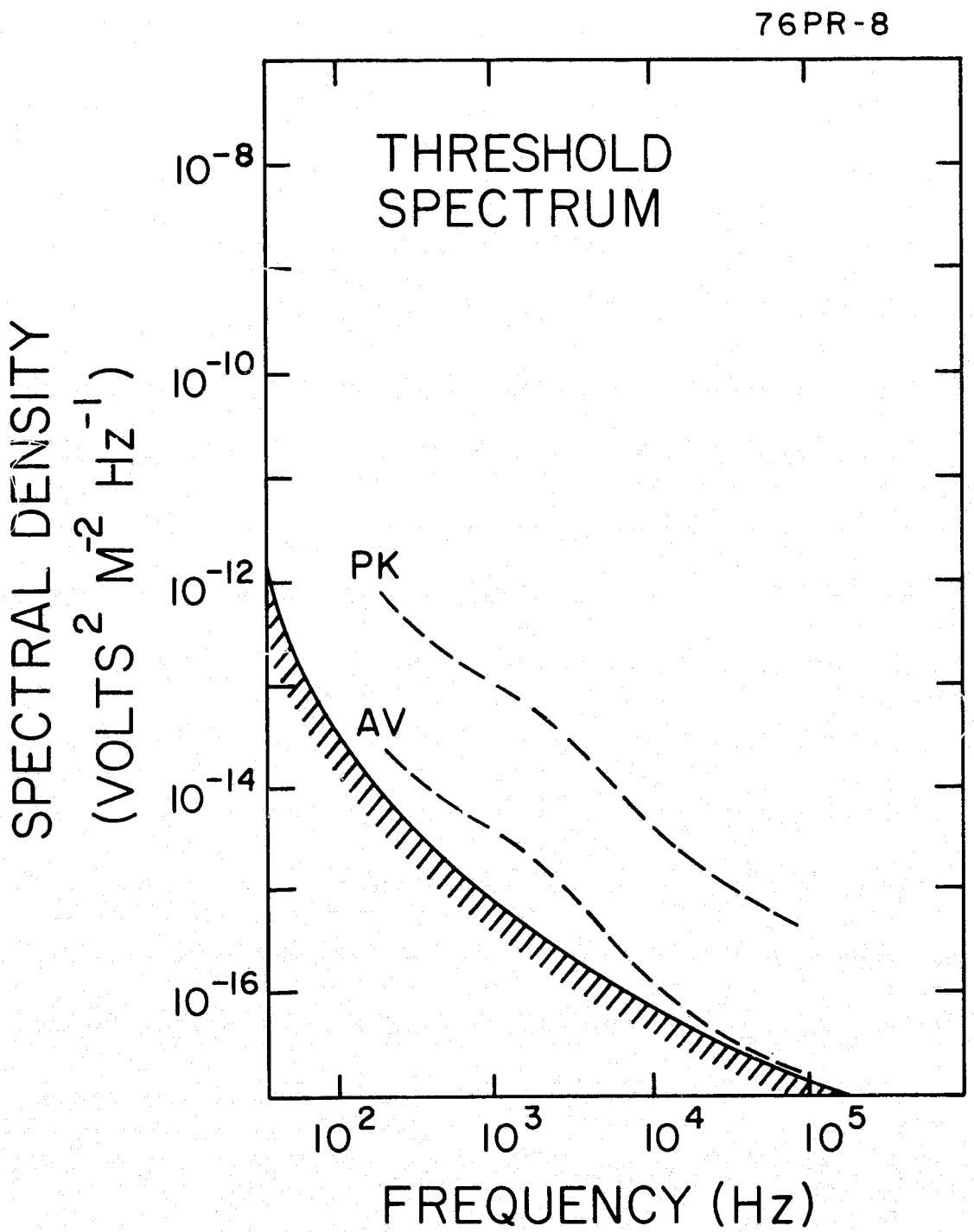
76PR-8
THRESHOLD
SPECTRUM
SPECTRAL DENSITY
(VOLTS^2 M^{-2} Hz^{-1})
10^{-8}
10^{-10}
10^{-12}
10^{-14}
10^{-16}
PK
AV
10^2
10^3
10^4
10^5
FREQUENCY (Hz)

Figure 2

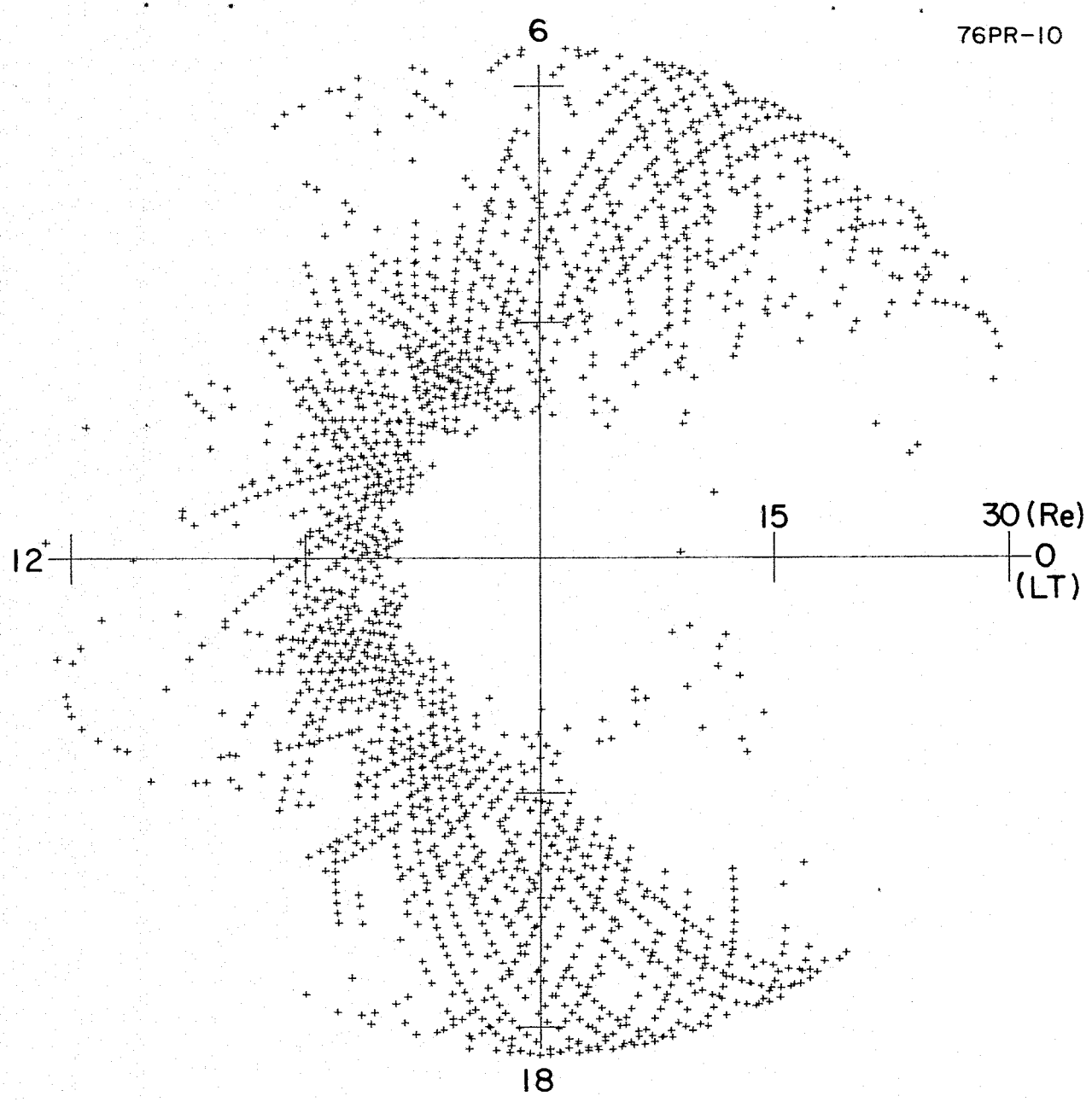

Figure 3

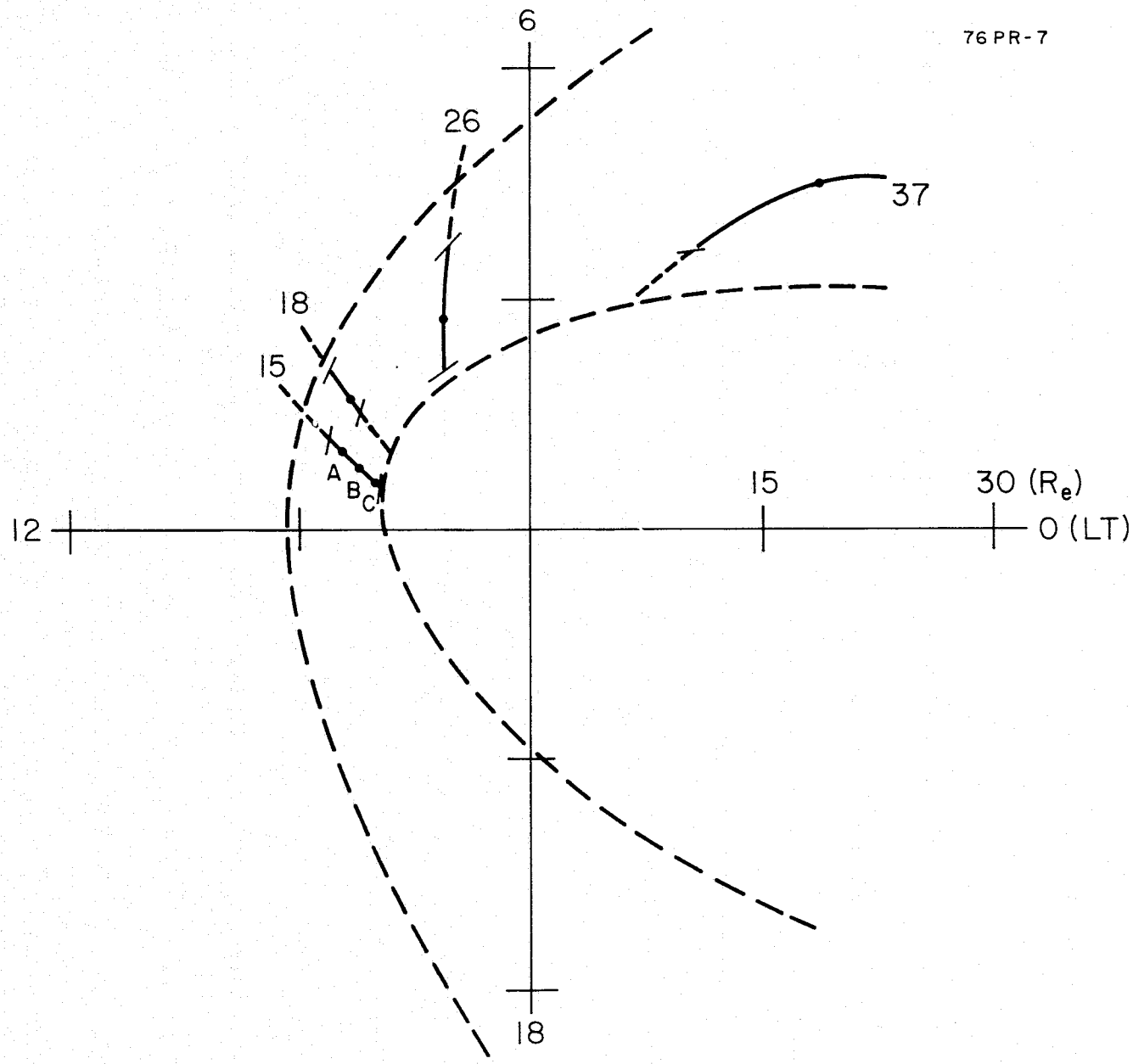

Figure 4

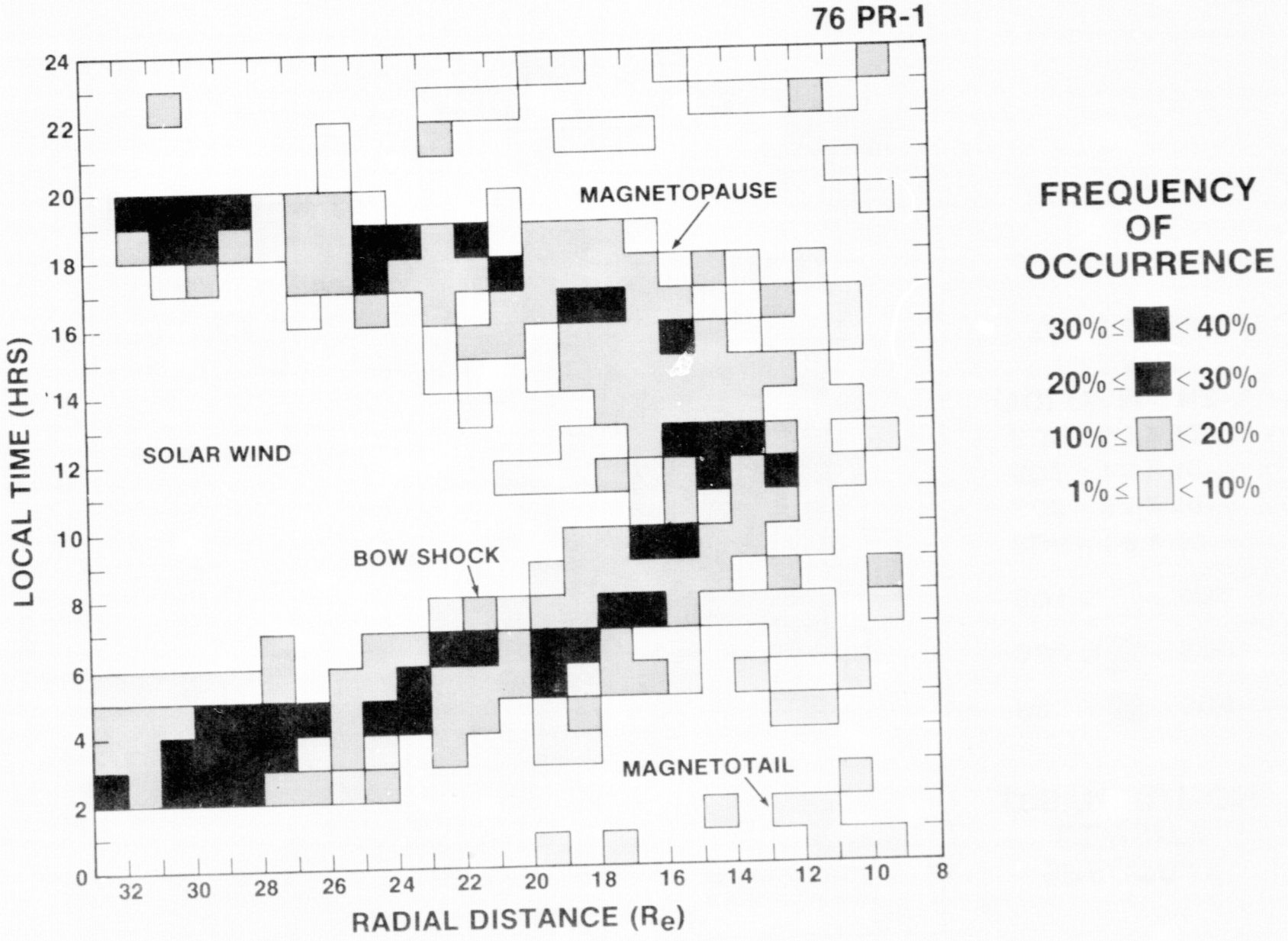
76 PR-1
MAGNETOPAUSE
SOLAR WIND
BOW SHOCK
MAGNETOTAIL
LOCAL TIME (HRS)
RADIAL DISTANCE (Re)
24
22
20
18
16
14
12
10
8
6
4
2
0
32
30
28
26
24
22
20
18
16
14
12
10
8
FREQUENCY OF OCCURRENCE
30% ≤ < 40%
20% ≤ < 30%
10% ≤ < 20%
1% ≤ < 10%

Figure 5

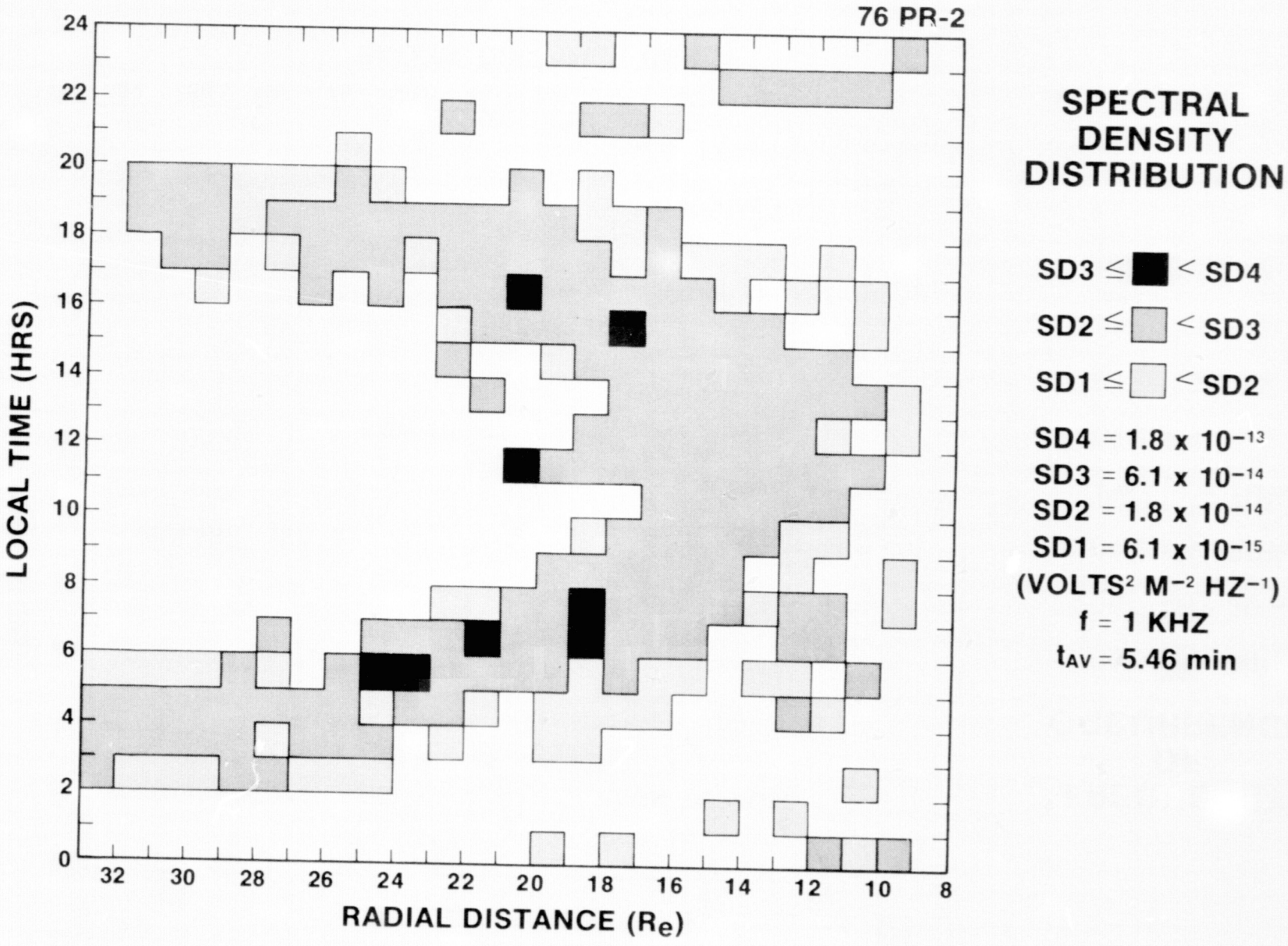
76 PR-2
LOCAL TIME (HRS)
RADIAL DISTANCE (Re)
SPECTRAL DENSITY DISTRIBUTION
SD3 ≤ ■ < SD4
SD2 ≤ ▒ < SD3
SD1 ≤ □ < SD2
SD4 = 1.8 x 10⁻¹³
SD3 = 6.1 x 10⁻¹⁴
SD2 = 1.8 x 10⁻¹⁴
SD1 = 6.1 x 10⁻¹⁵
(VOLTS² M⁻² HZ⁻¹)
f = 1 KHZ
tAV = 5.46 min

Figure 6

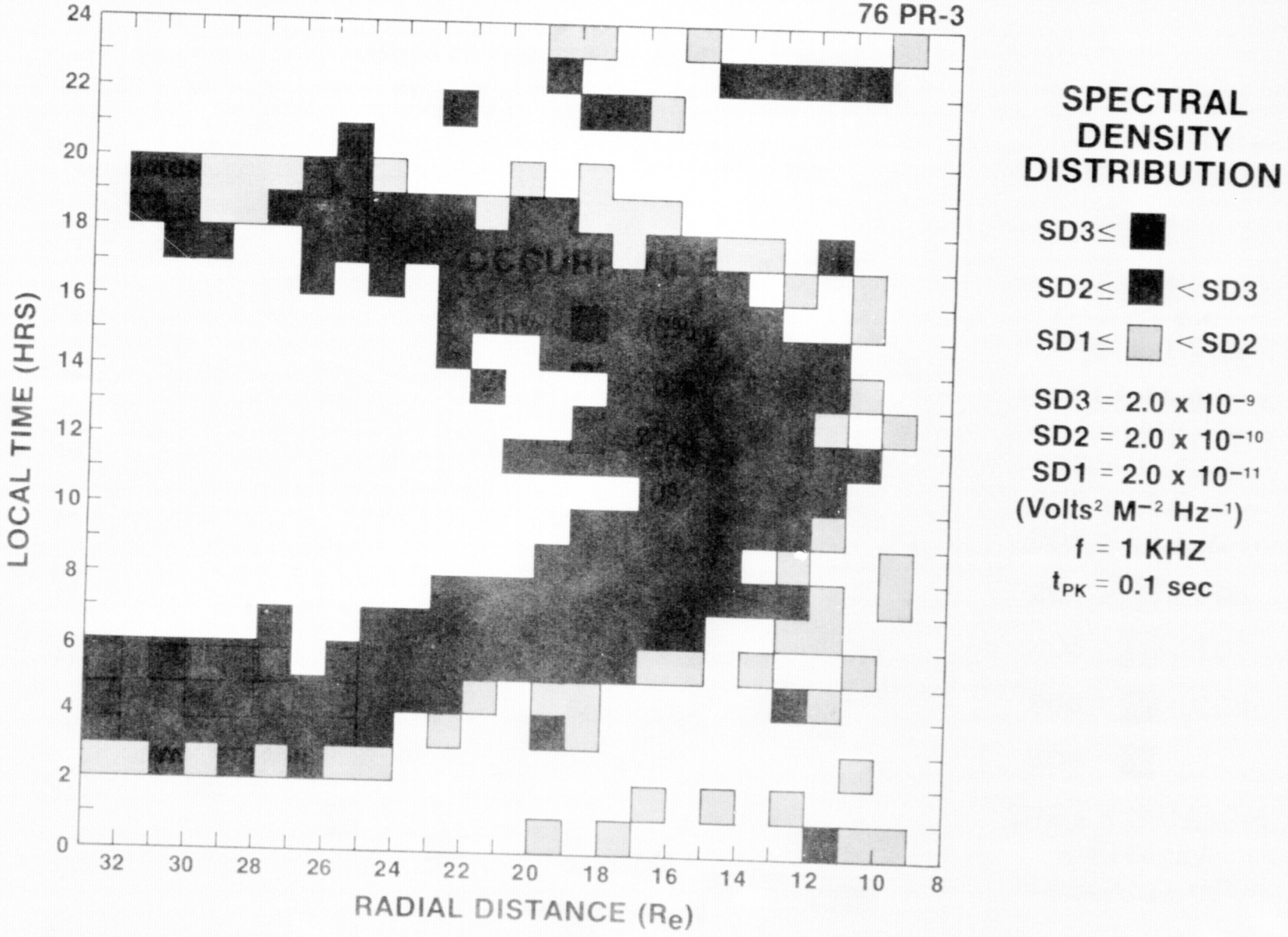
76 PR-3
LOCAL TIME (HRS)
RADIAL DISTANCE (Re)
24
22
20
18
16
14
12
10
8
6
4
2
0
32
30
28
26
24
22
20
18
16
14
12
10
8
SPECTRAL DENSITY DISTRIBUTION
SD3≤
SD2≤ < SD3
SD1≤ < SD2
SD3 = 2.0 x 10⁻⁹
SD2 = 2.0 x 10⁻¹⁰
SD1 = 2.0 x 10⁻¹¹
(Volts² M⁻² Hz⁻¹)
f = 1 KHZ
tPK = 0.1 sec

Figure 7

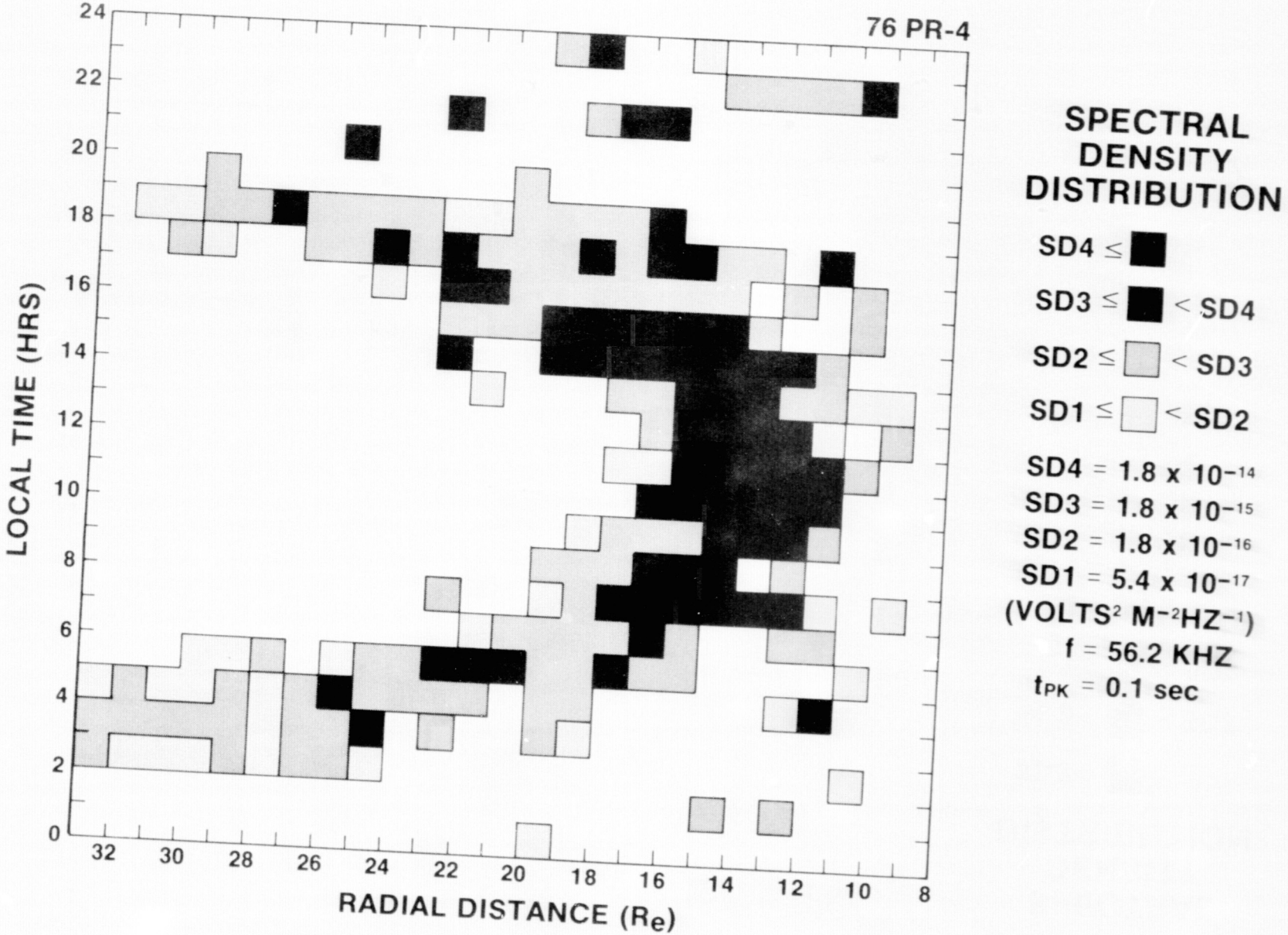
76 PR-4
LOCAL TIME (HRS)
RADIAL DISTANCE (Re)
24
22
20
18
16
14
12
10
8
6
4
2
0
32
30
28
26
24
22
20
18
16
14
12
10
8
SPECTRAL DENSITY DISTRIBUTION
SD4 ≤
SD3 ≤ < SD4
SD2 ≤ < SD3
SD1 ≤ < SD2
SD4 = 1.8 x 10⁻¹⁴
SD3 = 1.8 x 10⁻¹⁵
SD2 = 1.8 x 10⁻¹⁶
SD1 = 5.4 x 10⁻¹⁷
(VOLTS² M⁻²HZ⁻¹)
f = 56.2 KHZ
tPK = 0.1 sec

Figure 8

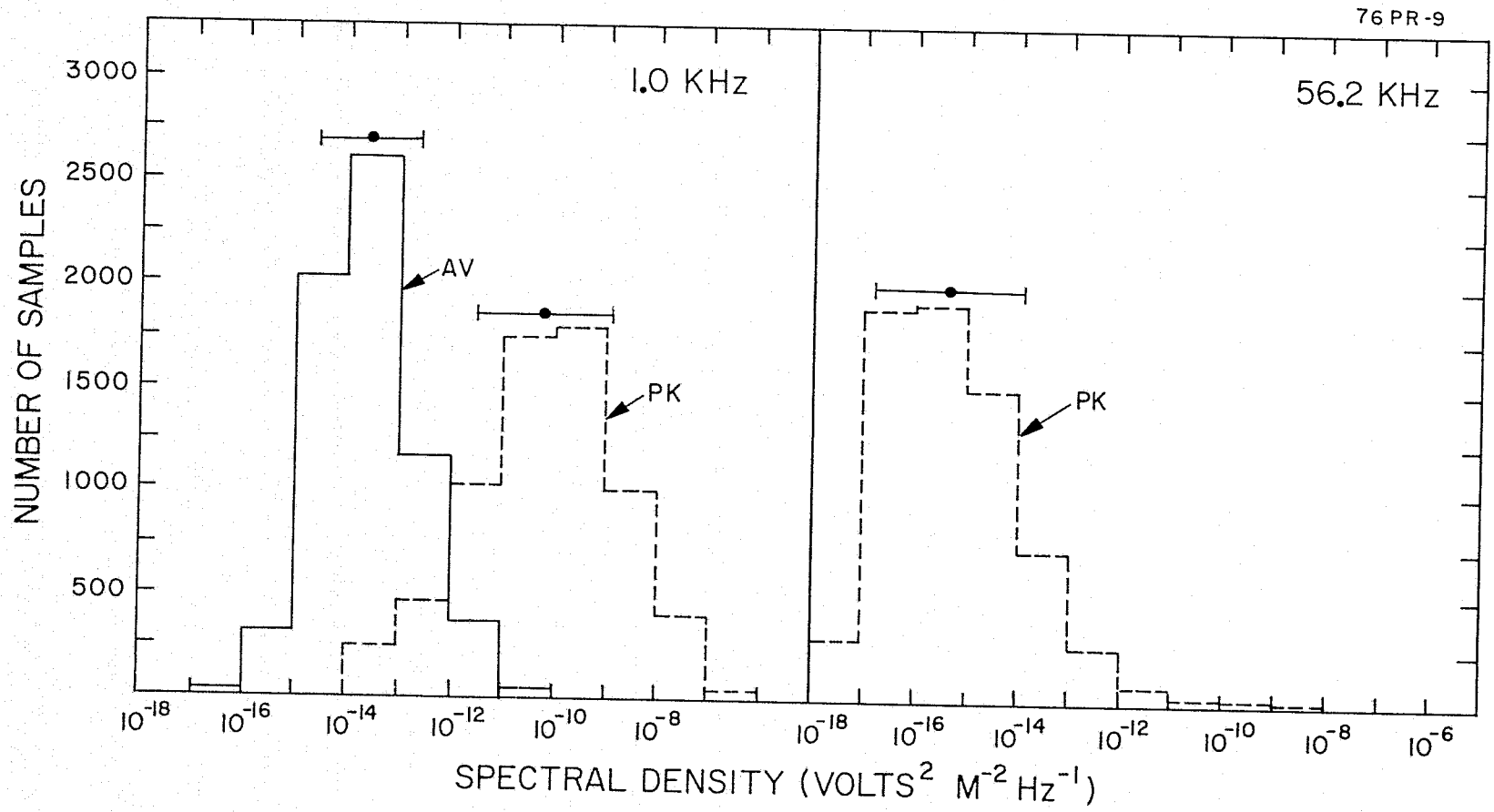
76 PR-9
1.0 KHz
56.2 KHz
AV
PK
PK
NUMBER OF SAMPLES
3000
2500
2000
1500
1000
500
10^{-18} 10^{-16} 10^{-14} 10^{-12} 10^{-10} 10^{-8}
10^{-18} 10^{-16} 10^{-14} 10^{-12} 10^{-10} 10^{-8} 10^{-6}
SPECTRAL DENSITY (VOLTS^2 M^{-2} Hz^{-1})

Figure 9

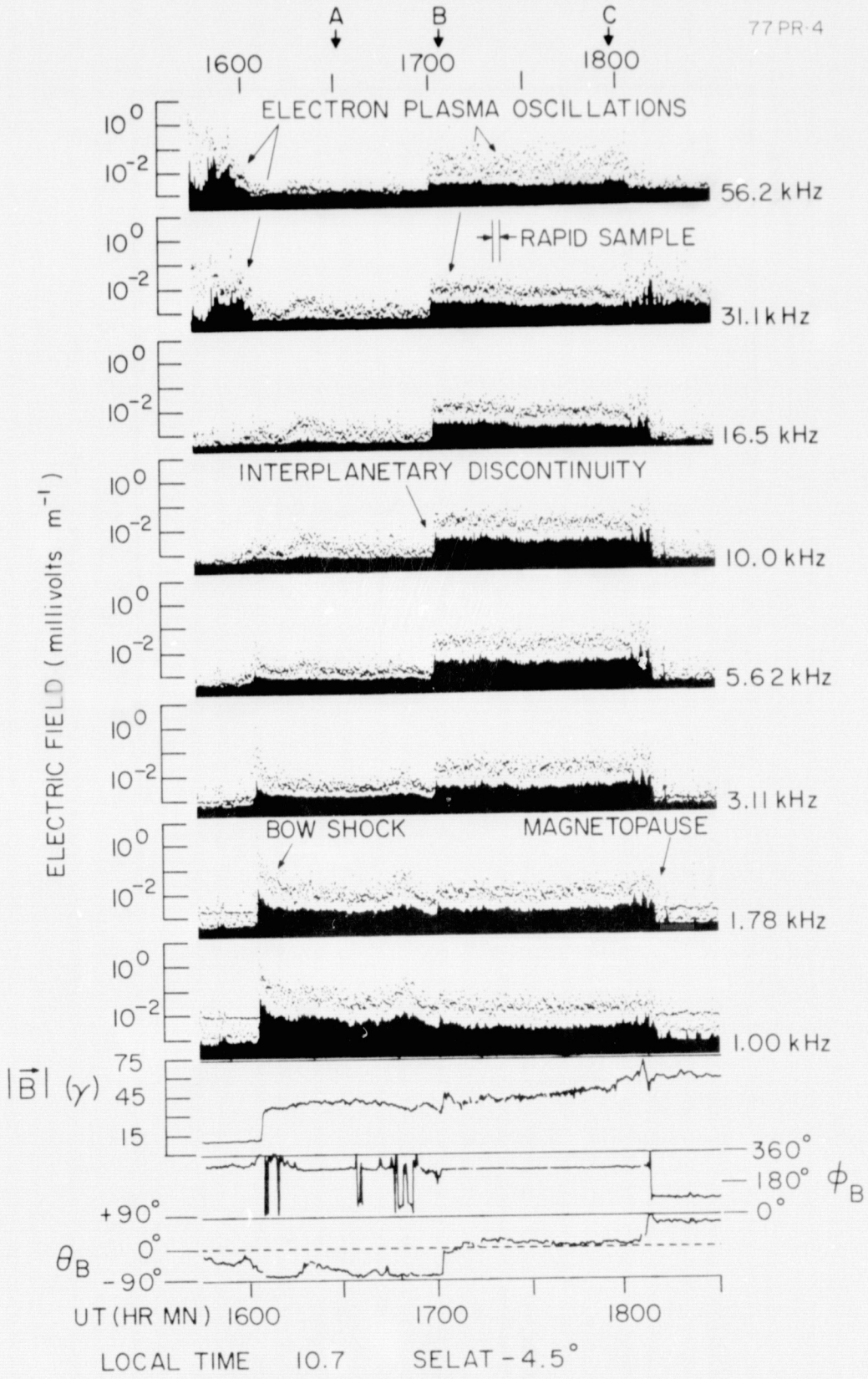
77 PR-4
A
B
C
1600
1700
1800
ELECTRON PLASMA OSCILLATIONS
RAPID SAMPLE
INTERPLANETARY DISCONTINUITY
BOW SHOCK
MAGNETOPAUSE
ELECTRIC FIELD (millivolts m⁻¹)
10⁰
10⁻²
56.2 kHz
31.1 kHz
16.5 kHz
10.0 kHz
5.62 kHz
3.11 kHz
1.78 kHz
1.00 kHz
|B| (γ)
75
45
15
360°
180°
0°
φB
+90°
0°
-90°
θB
UT (HR MN) 1600
1700
1800
LOCAL TIME 10.7
SELAT -4.5°

Figure 10

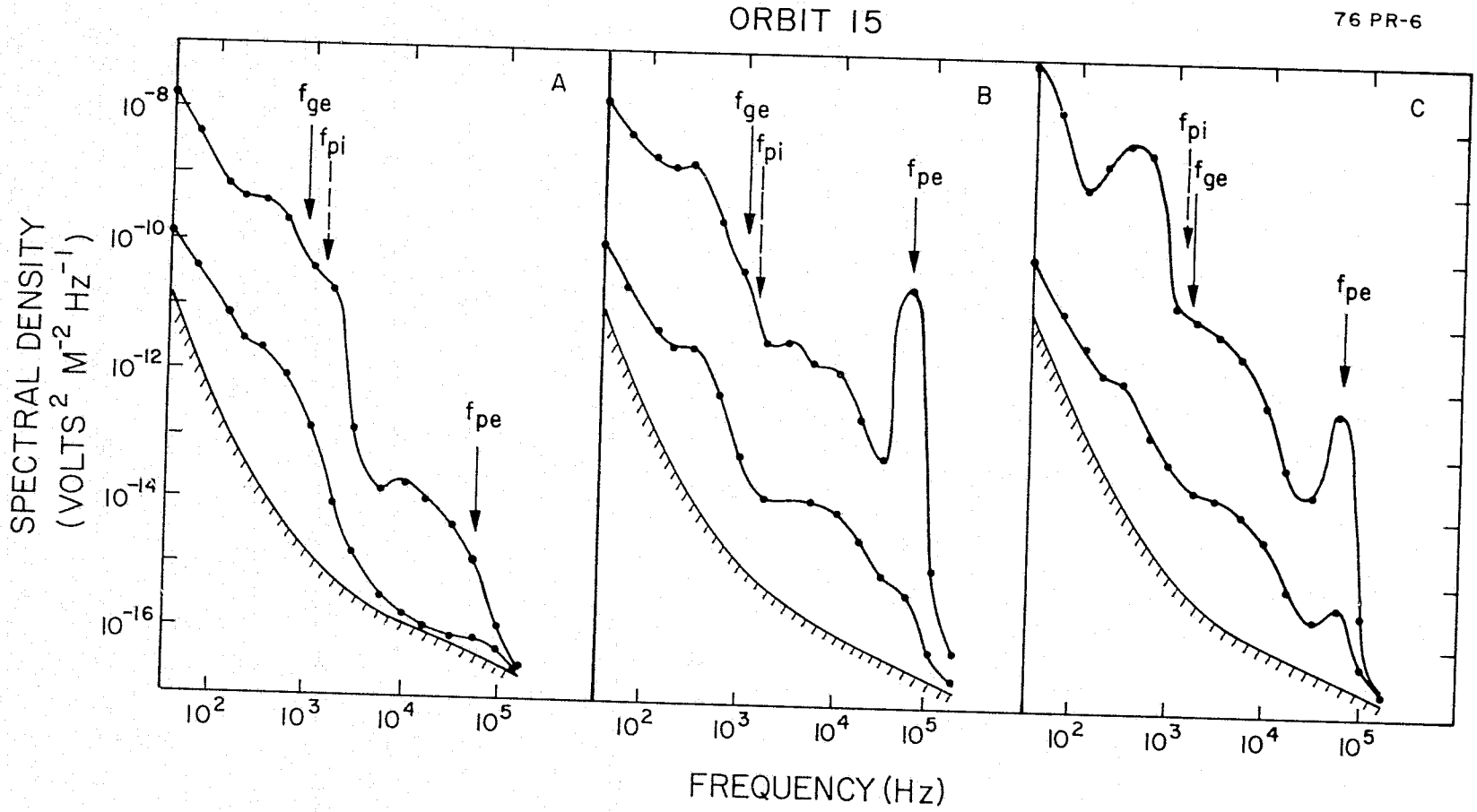
ORBIT 15
76 PR-6
A
B
C
f_{ge}
f_{pi}
f_{pe}
SPECTRAL DENSITY
(VOLTS^2 M^{-2} Hz^{-1})
10^{-8}
10^{-10}
10^{-12}
10^{-14}
10^{-16}
10^2
10^3
10^4
10^5
FREQUENCY (Hz)

Figure 11

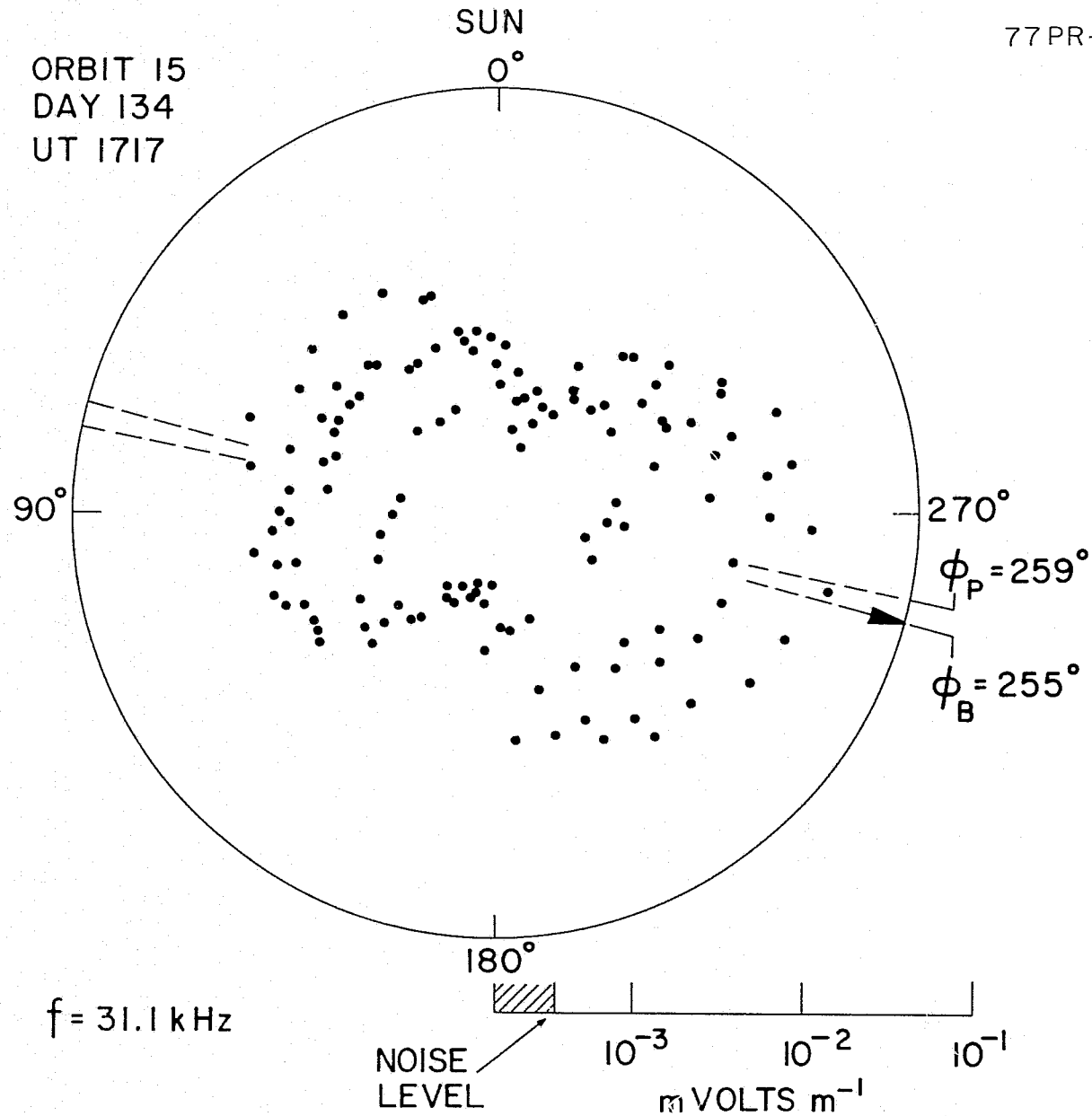
77PR-5
SUN
0°
ORBIT 15
DAY 134
UT 1717
90°
270°
$\phi_P = 259°$
$\phi_B = 255°$
180°
f = 31.1 kHz
NOISE
LEVEL
10^{-3}
10^{-2}
10^{-1}
mVOLTS m^{-1}

Figure 12

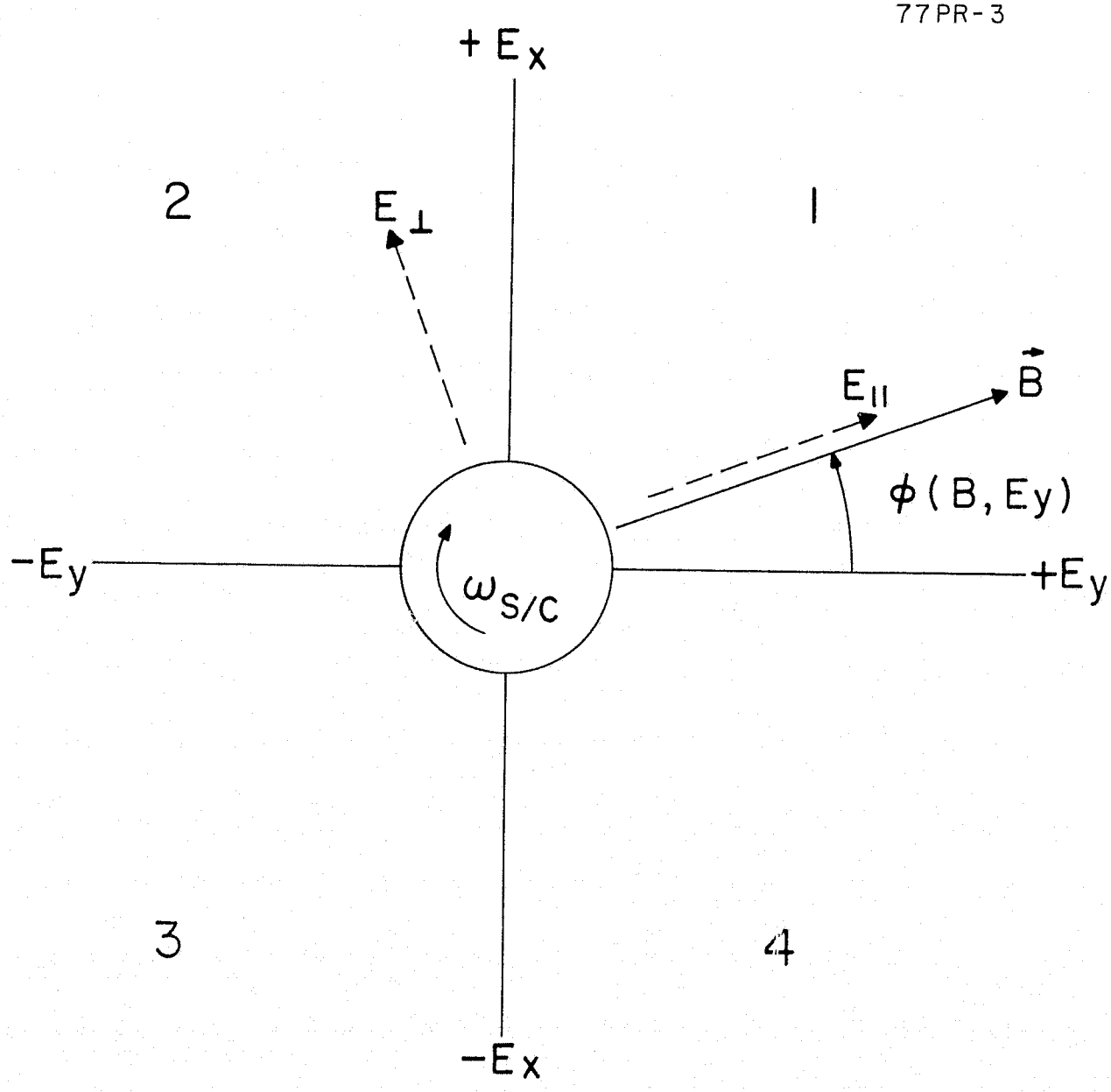

Figure 13

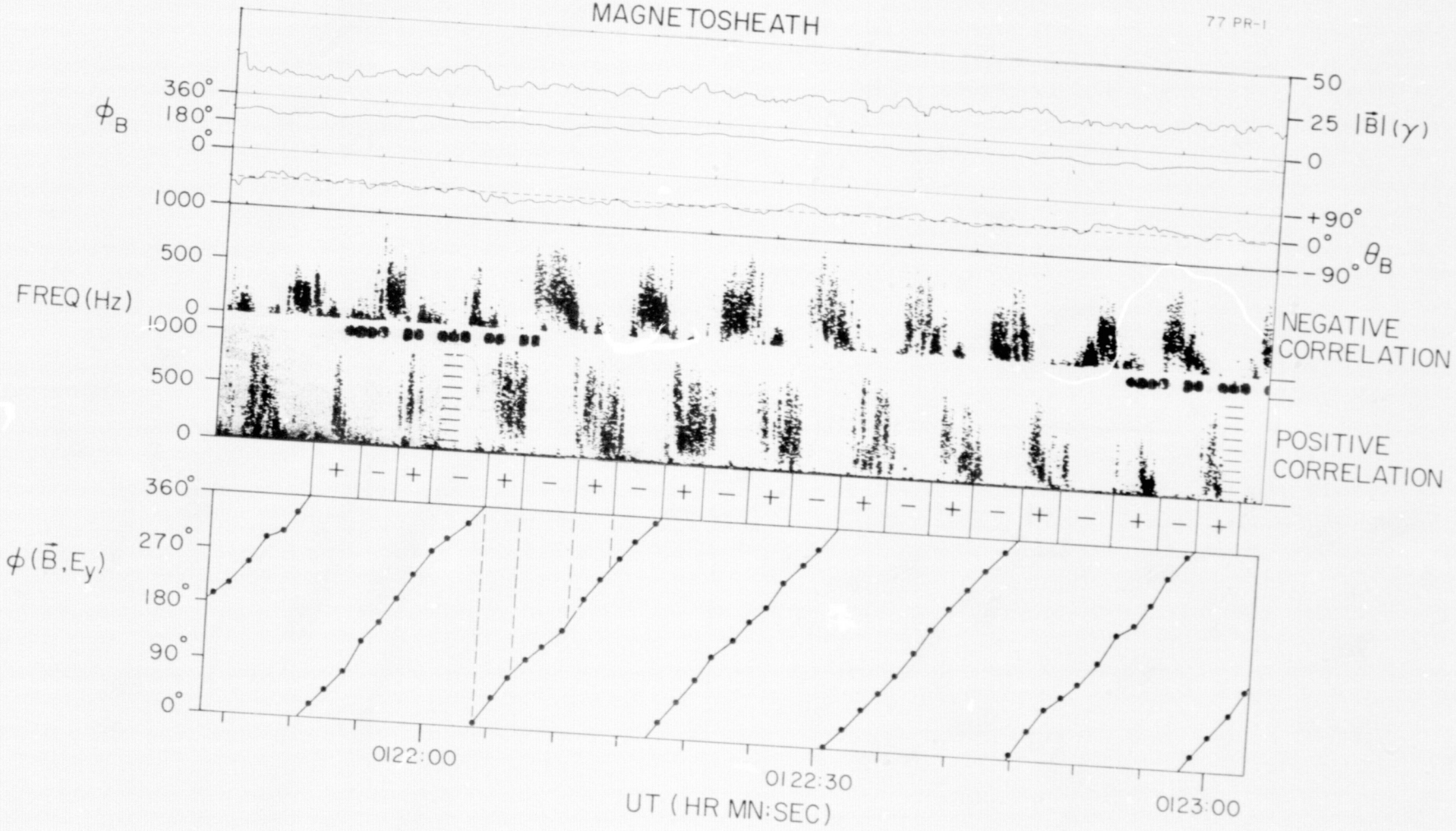
MAGNETOSHEATH
77 PR-1
ϕ_B
360°
180°
0°
50
25
$|\vec{B}|(\gamma)$
0
+90°
0°
−90°
θ_B
1000
500
0
FREQ (Hz)
1000
500
0
NEGATIVE CORRELATION
POSITIVE CORRELATION
+ − + − + − + − + − + − + − + − + − + − +
360°
270°
180°
90°
0°
$\phi(\vec{B}, E_y)$
0122:00
0122:30
0123:00
UT (HR MN:SEC)

Figure 14

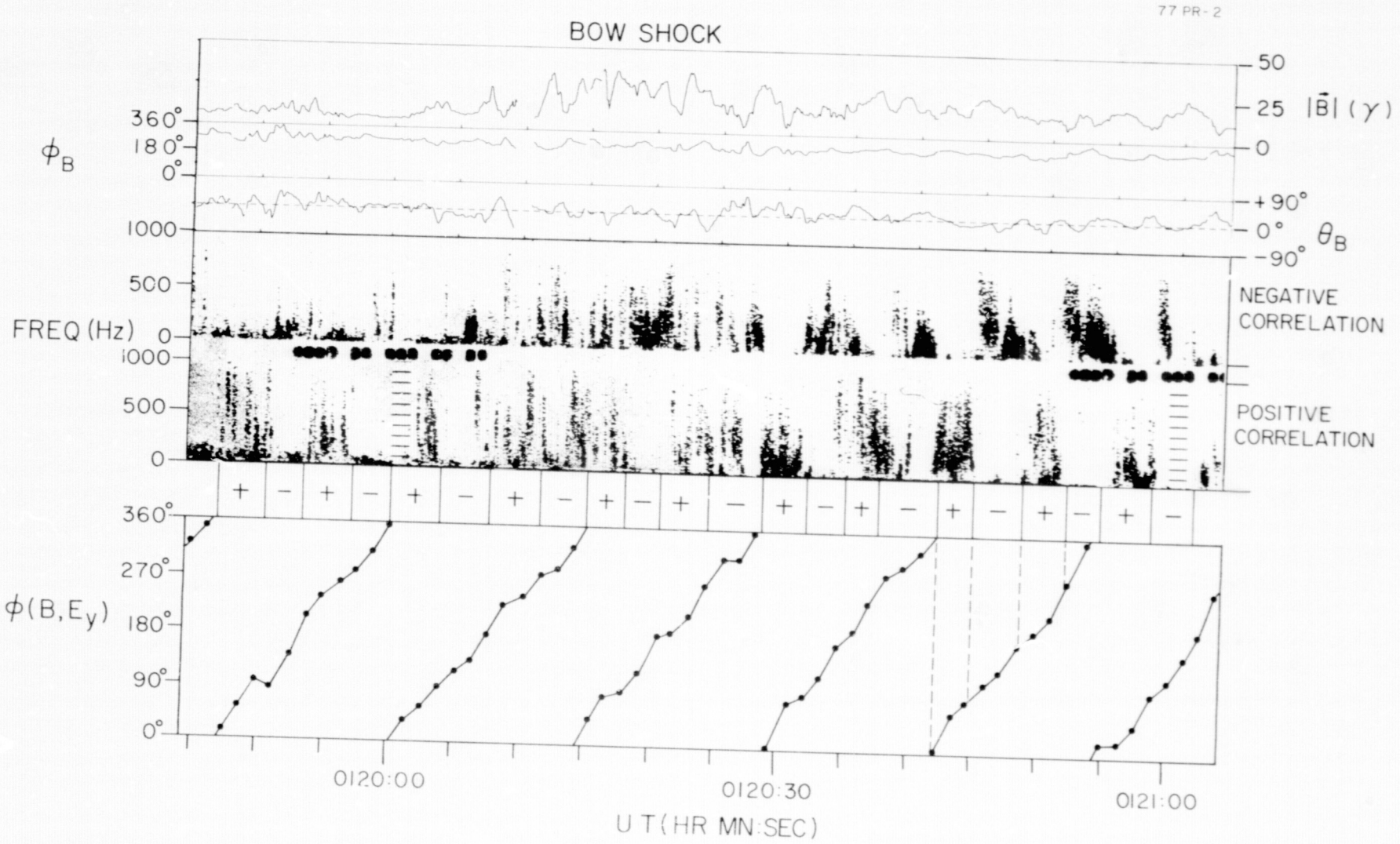
77 PR-2
BOW SHOCK
50
25
0
|B| (γ)
360°
180°
0°
φB
+90°
0°
−90°
θB
1000
500
0
FREQ (Hz)
1000
500
0
NEGATIVE CORRELATION
POSITIVE CORRELATION
+ − + − + − + − + − + − + − + − + − + − + − + −
360°
270°
180°
90°
0°
φ(B,Ey)
0120:00
0120:30
0121:00
UT (HR MN:SEC)

Figure 15